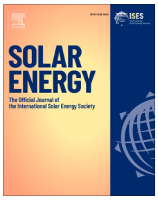
Solar Energy 313 (2026) 114585



Contents lists available at ScienceDirect

Solar Energy

journal homepage: www.elsevier.com/locate/solener





Thermal loss in concentrated solar power plants: A review of external and cavity receivers

Pedram Alamdari, Mehdi Khatamifar*, Wenxian Lin

College of Science & Engineering, James Cook University, Townsville, QLD 4811, Australia

ARTICLE INFO

Keywords:
Point-focus concentrated solar power systems
Convective thermal losses
Radiative thermal losses
Thermal efficiency
Receiver design

ABSTRACT

A vast solar resource remains underutilized, and cross-country comparisons show a persistent gap between high direct normal irradiation and realized solar generation. Concentrating solar power plants with external and cavity receivers can provide dispatchable, high temperature heat, but receiver performance is constrained by thermal losses. This review synthesizes loss mechanisms and evaluates models, experiments, and mitigation strategies across receiver types and operating regimes. Conduction through supports is typically negligible, contributing less than 1%, while convection ranges from a few to several tens of percent and increases with wind exposure and receiver orientation; radiation dominates above 500 °C because of its fourth-power dependence on temperature. External receivers incur higher losses than cavity receivers due to full ambient exposure and a larger sky view factor, whereas recessed cavity apertures reduce convective exchange and reradiation. We classify key design and operational levers, including aperture shaping and shielding, panelization, shaped geometries, internal fins and microchannels, air curtains, mass flow scheduling, and advanced materials such as low-emissivity coatings, aerogels, and phase change materials. Reported outcomes include up to 50% total loss reduction at 800 °C through coordinated geometry and surface optimization, multi-megawatt savings from partial dome shielding under moderate winds, and about 30% convective loss reduction from wind blocking and tuned air curtains. The review consolidates scattered evidence into a hierarchy that aligns interventions with the dominant loss pathway to improve receiver thermal efficiency.

1. Introduction

Rising population and industrial activity are driving rapid growth in electricity demand which, if met with fossil fuels, will further intensify global warming and air pollution. Renewable energy, particularly solar, provides a scalable alternative. The Earth receives about 4×10^6 exajoules of solar energy, far exceeding current and projected demand [1]. This potential could play a major role in improving electricity access, clean water availability, industrialisation, and food security worldwide [2].

Fig. 1 compares nine major economies ranked by Gross Domestic Product (GDP). Fig. 1(a) contrasts solar potential (left *y*-axis, average direct normal irradiation in kWh/m^2) with current utilization (right *y*-axis, solar electricity generation in PJ), quantifying the gap between available resources and generation. Fig. 1(b) relates fossil fuel production (left *y*-axis, PJ) to GDP (right *y*-axis, trillion USD), linking economic scale, reliance on conventional energy, and renewable deployment.

China and the United States generate the largest absolute amounts of solar electricity, reflecting their large economies, capital markets, and transmission grids. Because utility-scale solar plants require substantial upfront investment, deployment correlates more strongly with GDP than with direct normal irradiation (DNI). As a result, high-DNI countries such as Chile and South Africa can show lower absolute solar generation than wealthier countries with lower DNI. Wealth is not sufficient, however: Australia, despite having a higher GDP than Spain, produces roughly 16% less solar electricity, indicating the additional influence of resource endowments, fossil-fuel availability and legacy infrastructure, as well as policy, market design, and grid integration.

Among solar technologies, concentrating solar power (CSP) is attractive because it is dispatchable, compatible with hybrid operation, naturally integrates thermal-energy storage, and can be cost-effective [6–8]. Fig. 2 shows four CSP types. In linear CSP systems (Fig. 2(a),(b)), parabolic trough and linear Fresnel collectors focus solar flux along a line, and the heat transfer fluid (HTF) is heated in a linear receiver. In point-focus systems (Fig. 2(c),(d)), mirrors concentrate radiation at a focal point, and the HTF extracts heat from an external or cavity receiver mounted on a tower or parabolic dish.

* Corresponding author.
Email address: mehdi.khatamifar2@jcu.edu.au (M. Khatamifar).

https://doi.org/10.1016/j.solener.2026.114585
Received 13 November 2025; Received in revised form 26 March 2026; Accepted 30 March 2026
Available online 16 April 2026
0038-092X/© 2026 The Authors. Published by Elsevier Ltd on behalf of International Solar Energy Society. This is an open access article under the CC BY license (http://creativecommons.org/licenses/by/4.0/).

Nomenclature

Parameters

Q	Heat flux, W/m^2
T	Temperature, K

Subscripts

abs	Absorber
amb	Ambient
cond	Conductive heat transfer
conv	Convective heat transfer
HTF	Heat transfer fluid
in	Incident
rad	Radiative heat transfer
T	Total

By 2050, CSP is projected to supply 11% of global electricity, about 954–1080 GW [11]. Fig. 3 combines a global DNI map [3] with a market segmentation chart [12] comparing installed or commissioned CSP projects by receiver technology. Beyond the 6418.16 MW operational CSP capacity (including hybrid systems), 2464 MW is under construction, led by China, Spain, and the USA. Within this pipeline, external and cavity receivers account for about 65% of capacity under construction, compared with about 23% in operating plants, indicating a shift toward high-flux tower and cavity receivers that concentrate flux at a point and benefit from improved thermal management relative to parabolic trough, dish, and linear Fresnel systems.

As CSP deployment grows, particularly for systems with external and cavity receivers, improving receiver thermal efficiency is a central priority. Reducing heat loss by controlling conduction, convection, and radiation increases efficiency and lowers operating costs [13]. In point-focus CSP, losses occur through conduction, convection, and radiation. Conduction is mainly through structural supports and is typically negligible in well-designed receivers, often $< 1\%$ of total losses [14,15]. Convection arises from buoyancy and wind and may be mixed. Radiation dominates at high temperatures, typically above 500 °C, consistent with the Stefan–Boltzmann law.

Foundational cavity receiver loss studies were reported by Clausing and co-workers [16–18] and by Harris and Lenz [19]. For external receivers, Sandia National Laboratories studies in the mid-1980s established thermal loss characteristics for exposed cylindrical and flat surfaces [20–22]. Existing reviews cover CSP technologies, receiver concepts, modeling approaches, and selected mitigation strategies; however, evidence remains fragmented in how losses are compared across external versus cavity receivers and operating regimes (wind exposure, tilt/yaw conventions, and non-uniform flux). Consequently, it is often unclear which mitigation levers are most effective for a given temperature, geometry, and environment, and why quantitative trends differ across studies.

This review provides a mechanism-based synthesis to make cross-study comparisons actionable. First, we present a unified framework separating (i) loss mechanisms and drivers and (ii) mitigation strategies (Fig. 7), distinguishing controlling variables from correlates. Second, we consolidate experimental and numerical results into comparable ranges for convective and radiative losses across receiver types and regimes, emphasizing wind exposure, orientation, and temperature. Third, we map practical levers (geometry, surfaces/materials, and operational control) to the dominant loss pathway in each regime. Distinctions from prior reviews and remaining gaps are summarized in Section 8.

2. Classification of CSP systems

As shown in Fig. 2, CSP systems are grouped into four primary types, two point-focus and two linear-focus. Performance depends on both design and intrinsic characteristics. Table 1 shows that point-focus systems reach higher operating temperatures than linear systems because they use higher concentration ratios, the ratio of solar flux at the absorber to the incident flux [23]. These higher temperatures enable applications beyond electricity generation, including hydrogen production [24,25] and solar thermochemical energy storage [26]. Point-focus systems therefore offer distinct receiver options for high temperature solar applications.

As depicted in Figure Fig. 4, external receivers are commonly cylindrical (or semi-cylindrical), star shaped, or flat (billboard) [28–31]. In cylindrical receivers, the surface faces the heliostat field and multiple tubes are arranged around a polyhedral form. Approximately half of each tube surface is directly irradiated while the HTF removes energy from the uninsulated side and the remaining half is insulated. Tubes use solar absorber coatings, with high temperature silicone-based paints widely adopted. Recent work reports hierarchical coatings [32,33] and scalable nanostructures [34] that increase solar absorption and improve durability. Flat receivers, irradiated from a narrower range of directions, mount several vertical tubes on a surface or combine vertical and horizontal tubes in intersecting layouts [30]. As with cylindrical receivers, roughly half the tube area absorbs solar flux. Geometrical modifications, including star-shaped and bladed concepts, promote more uniform flux and lower heat loss [31].

Cavity receivers are also widely used in tower-based CSP. As with external designs, they employ multiple vertical tubes arranged as a polyhedral structure, but the tubes are enclosed by insulated walls and solar radiation enters only through an aperture, which reduces thermal losses [35]. Other cavity geometries, including conical, hemispherical, and cylindrical cavities, follow the same principle [36]. As shown in Fig. 5, a tube is formed into a cylindrical, conical, or hemispherical path so that reflected flux enters the cavity and is absorbed by the tube, while the external surface is insulated.

3. Thermal loss mechanisms

As shown in Fig. 6, thermal losses in point-focus receivers are convective, radiative, and conductive. The large temperature difference between receiver surfaces and ambient air drives convection that removes part of the absorbed solar energy. Because receiver temperatures are high (Table 1), radiative exchange with the surroundings is also significant. Conduction through structural elements, mounts, and supports carries away additional heat. The energy balance is

$$Q_{\text{Solar,in}} = Q_{\text{HTF}} + Q_{\text{T,loss}}, \tag{1}$$

$$Q_{\text{T,loss}} = Q_{\text{rad,abs-amb}} + Q_{\text{conv,abs-amb}} + Q_{\text{cond,support}}, \tag{2}$$

where $Q_{\text{Solar,in}}$ is the incident solar power on the receiver, Q_{HTF} is the thermal power transferred to the HTF, $Q_{\text{T,loss}}$ is the total heat loss, $Q_{\text{rad,abs-amb}}$ is the net radiative heat flux from the absorber to the ambient, $Q_{\text{conv,abs-amb}}$ is the convective heat flux from the absorber to the ambient, and $Q_{\text{cond,support}}$ is the conductive heat flux from the absorber through holders and fixtures.

For external receivers, $Q_{\text{rad,abs-amb}}$ and $Q_{\text{conv,abs-amb}}$ denote radiative and convective exchange from fully exposed absorber surfaces to the ambient. For cavity receivers, these terms are governed mainly by aperture-mediated radiative escape and air exchange through the aperture, rather than by direct ambient sweeping over the absorber.

In cavity receivers, the recessed absorber exchanges heat with the environment primarily through the aperture. Radiative loss is reduced because the effective absorber-to-ambient view factor is smaller and much of the emitted radiation is intercepted by the cavity interior and reabsorbed after one or more reflections (the “cavity effect”). Convective

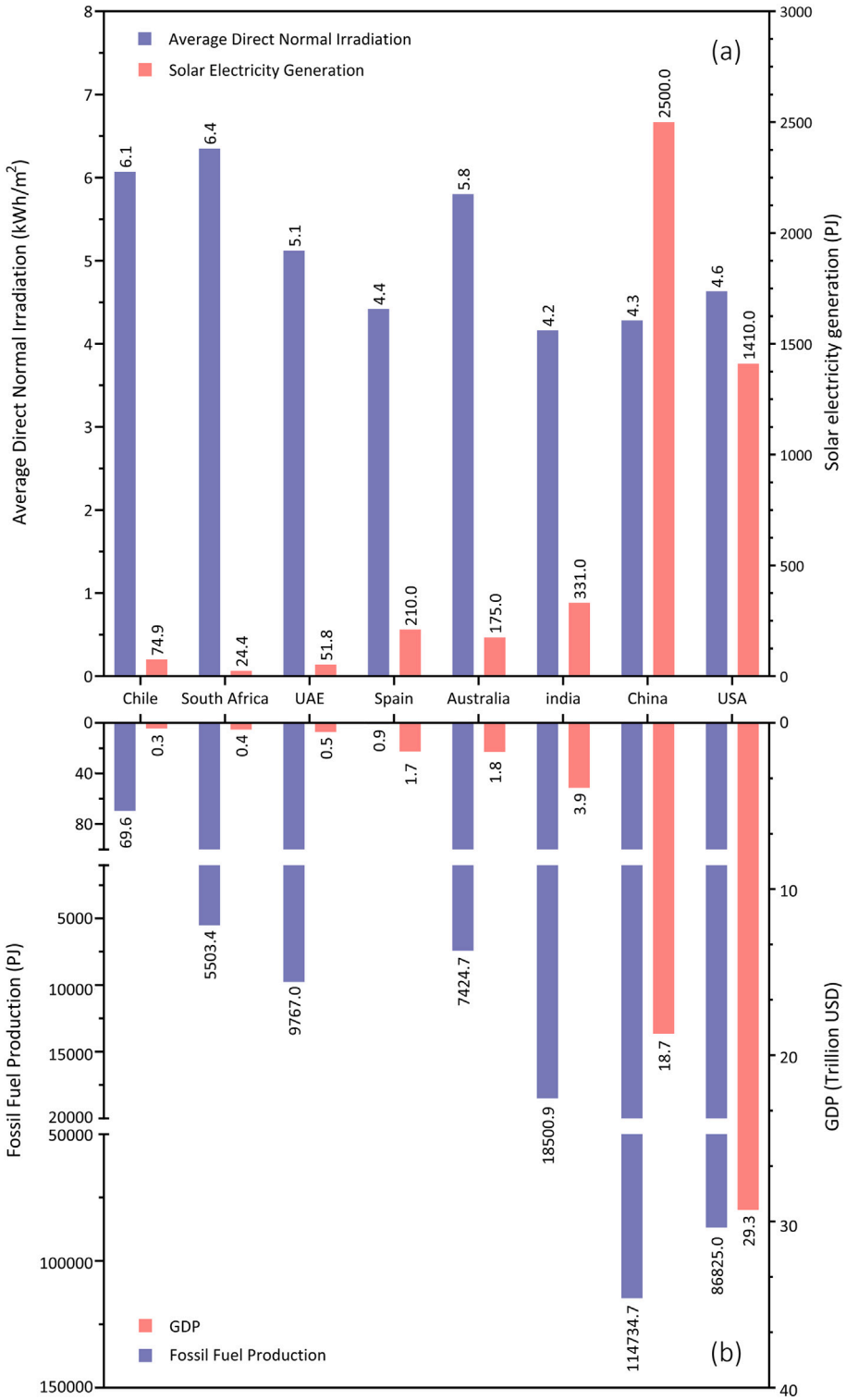


Fig. 1. Comparison of solar electricity generation, fossil fuel production, and GDP: (a) solar generation and average DNI, (b) GDP and fossil fuel production. (Data from Refs. [3–5]).

loss is also lower because ambient air does not freely sweep the absorber; instead, heat removal is dominated by buoyancy-driven inflow/outflow through the aperture (natural convection) and, under wind, by pressure-driven aperture pumping (mixed/forced exchange). When conduction through supports and insulation is small, these aperture-controlled radiative and convective mechanisms dominate total loss, explaining the systematically lower losses of cavity designs relative to fully exposed external receivers.

At high temperatures, radiation often dominates because radiative transfer scales with the fourth power of absolute temperature. Geometry and exposure strongly modulate losses: external receivers experience higher convective and radiative losses because absorber tubes are fully exposed to ambient air and wind (enhancing forced convection) and have a larger effective view factor to the sky, whereas cavity designs reduce the absorber–ambient view factor and restrict most convective exchange to the aperture.

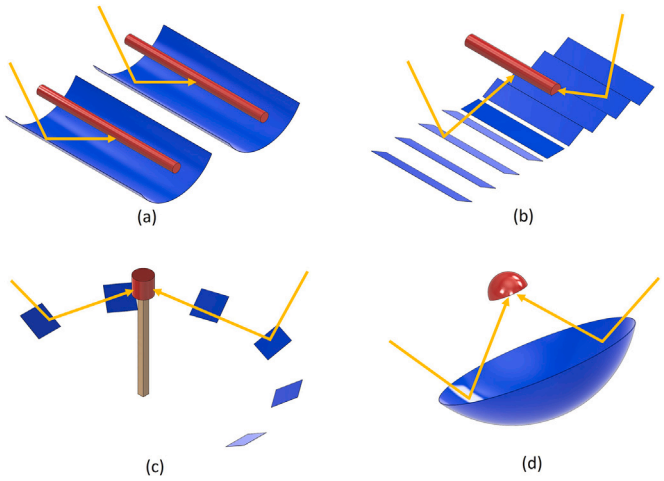


Fig. 2. Types of CSP systems: (a) parabolic trough collectors, (b) linear Fresnel collectors, (c) external receiver central towers, (d) cavity receivers. (Adapted from [6,9,10]).

4. Existing reviews involving point-focused CSPs

Over the past decade, numerous reviews have addressed CSP systems [27,35–40]. For power-tower, point-focus CSP, prior work has examined heliostat field layouts [41], economic feasibility, heliostat calibration and tracking [42–44], cylindrical receiver service life [45], and surface coatings [46].

For dish-Stirling systems, Zayed et al. [47] and Malik et al. [48] focused on design criteria, thermal and thermodynamic behavior, and applications. Conroy et al. [49] and Merchan et al. [50] analyzed receiver performance from thermomechanical and system perspectives, while Jafrancesco et al. [51] and Lipinski et al. [52] compared simulation tools and heat transfer mechanisms. Milidonis et al. [53] and He et al. [54] investigated artificial intelligence and nonuniform flux distribution in point-focus CSP.

Regarding receiver geometry and working media, Kumar et al. [55] compared cavity configurations, and Nandanwar and Walke [56] reviewed geometric optimization, heat transfer fluids (HTFs), and phase change material (PCM) integration in parabolic dish cavities. Avila-Marín et al. [57] assessed porous structures in volumetric absorbers and clarified their role in enhancing internal heat transfer and optical–thermal coupling. In the HTF domain, Coventry et al. [58] evaluated sodium configurations and concluded that performance gains outweigh associated risks, Aljaerani et al. [59] extended this to nanofluid-enhanced molten salts, and Liu et al. [60] and Lambrecht et al. [61] provided molecular dynamics insights for molten chloride systems.

From a thermal loss perspective, Kasaeian et al. [36] analyzed cavity geometries using thermal and exergy assessments and identified thermal loss as a critical parameter. Hanrieder et al. [62] synthesized atmospheric attenuation models, and Samanes et al. [63] compared natural convection correlations. Abed et al. [64] and Wasankar and Gulhane [65] reviewed design modifications and strategies to reduce thermal losses in parabolic dish systems.

Table 2 summarizes how these reviews treat receiver parameters in point-focus CSP. Considering point-focus systems through the lens of heat loss, beyond geometry or HTF selection alone, provides a complementary route when direct efficiency gains are limited, because targeted loss mitigation can indirectly raise overall efficiency. This motivates further study, consistent with Alamdari et al. [66], who call for more detailed investigations of thermal losses in point-focus CSP.

Summarizes how existing reviews treat receiver-related parameters in point-focus CSP and reveals two gaps. First, most reviews emphasize either system-level design (heliostats, plant economics, lifetime) or a single receiver class, and thus lack a consistent side-by-side treatment of external and cavity receivers under comparable operating descriptors (wind exposure, orientation, and flux non-uniformity). Second, mitigation strategies are often catalogued qualitatively, without specifying the conditions under which a given strategy is effective (e.g., convection-dominated versus radiation-dominated regimes).

Accordingly, this review differs by (i) introducing a unified framework that separates efficiency parameters from loss drivers and mitigation options (Fig. 7), (ii) consolidating reported loss magnitudes and mitigation outcomes into comparable ranges across receiver types and regimes, and (iii) mapping practical interventions to the dominant loss pathway to form a hierarchy of design levers. We also identify barriers to reliable cross-study synthesis, especially inconsistent reporting of environmental and boundary conditions, and highlight the need for coordinated in situ experiments and coupled modeling to reduce uncertainty and improve transferability.

5. Classification of thermal losses research

Analysis of CSP receiver performance indicates two complementary routes to improvement: enhancing thermal efficiency through operational and design parameters and reducing heat losses by understanding and mitigating their mechanisms. As illustrated in Fig. 7, these routes can be grouped into three interrelated domains: thermal efficiency parameters, loss mechanisms and drivers, and mitigation strategies, each containing variables that influence receiver performance in point-focus systems.

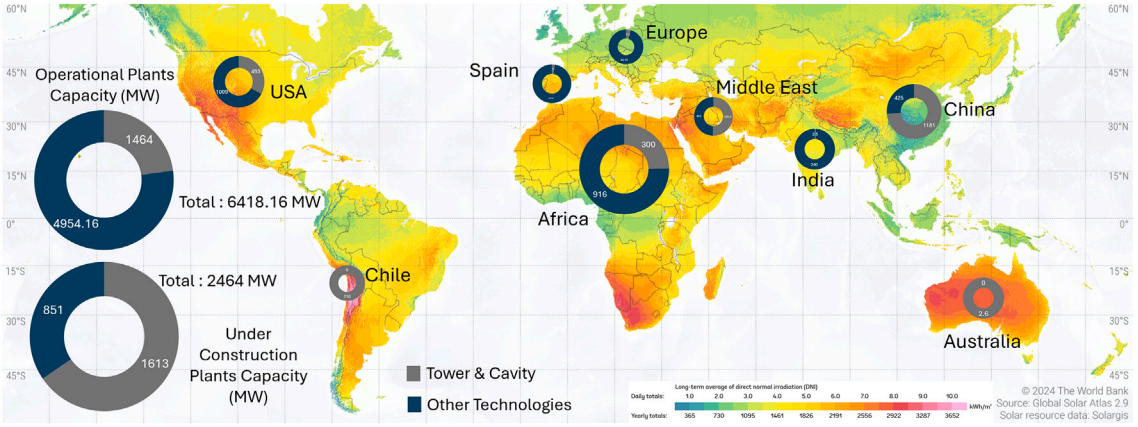


Fig. 3. CSP projects worldwide, comparing tower and cavity receivers with other CSP receiver technologies. (Data from [12]; solar irradiation map adapted from [3]).

Table 1
Comparison of different CSP technologies [12,27].

CSP Type	Normal Capacity (MW)	Operating Temperature (°C)	Concentration Ratio	Solar to Electricity Efficiency (%)
Parabolic trough	Up to 600	Up to 550	30–80	Up to 16
Linear Fresnel	Up to 125	Up to 550	30–80	Up to 12
Cavity receiver	Parabolic dish: Up to 1.5 / tower-mounted: Up to 20	Up to 1500	1000–3000	Up to 29
External receiver	Up to 377	Up to 1200	200–1000	Up to 22

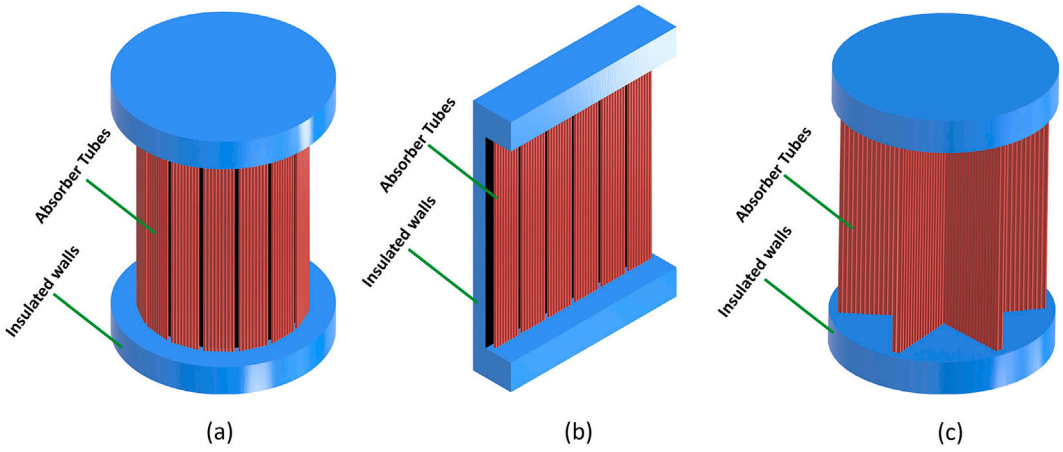


Fig. 4. External receivers: (a) cylindrical receiver, (b) flat billboard receiver, (c) star-shaped receiver.

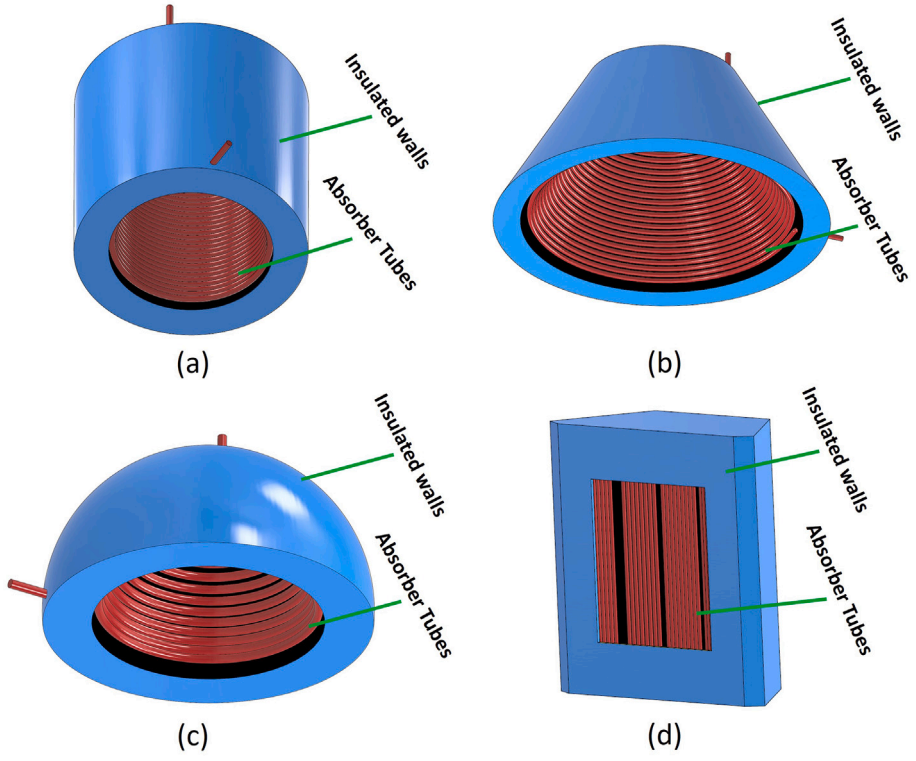


Fig. 5. Cavity receivers: (a) cylindrical cavity, (b) conical cavity, (c) hemispherical cavity, (d) tower-mounted cavity.

Category 1: Thermal efficiency parameters. This category includes factors that directly govern receiver output without primarily altering loss mechanisms. Key variables are operating temperature, HTF mass flow rate, solar incident flux, concentration ratio, and receiver configuration (cavity or external). Joint optimization of these parameters complements loss mitigation and together they determine overall thermal efficiency.

Category 2: Loss mechanisms and drivers. This category covers convection, conduction, and radiation and the factors that govern them. Conductive losses are determined by structural configuration and

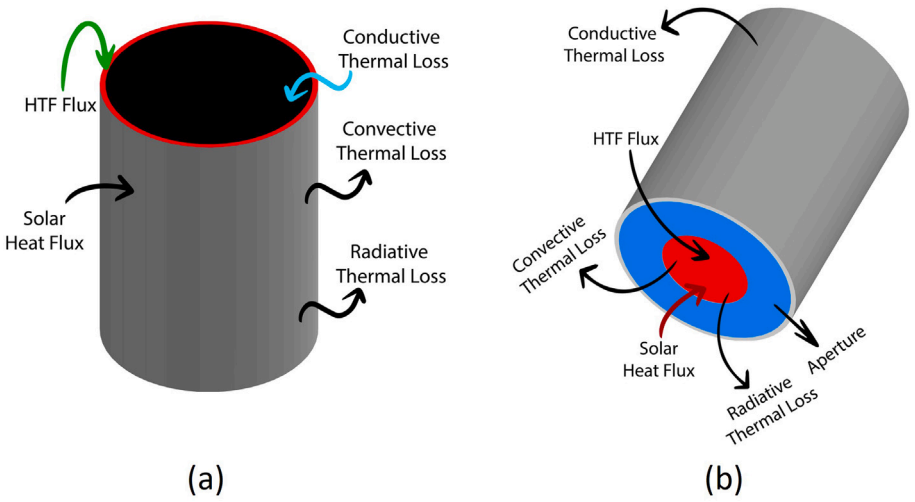


Fig. 6. Heat losses of point-focused CSPs: (a) external receiver and (b) cavity receiver.

Table 2
Comparison with other relevant reviews.

Reference	Thermal & Optical Performance	Safety, Mechanical & LCA	Thermal loss
[36]	Cavity	—	—
[37]	Cavity	—	—
[43]	Cavity	—	—
[49]	Cavity	—	—
[46]	External	—	—
[44]	Both	—	—
[45]	Both	Both	—
[47]	Both	—	—
[48]	Both	Both	—
[55]	Both	—	—
[35]	—	Both	—
[51]	—	—	Cavity
[53]	—	—	Cavity
[52]	Cavity	—	Cavity
Current Study	—	—	Both

Cavity: focusing on cavity receivers.
External: focusing on external receivers.
Both: focusing on both cavity & external receivers.

insulation and, in well-designed receivers, are small compared with convective and radiative losses. Geometry differentiates receiver types. Cavity receivers, with recessed absorbers, develop stagnation zones that limit exchange with ambient air and reduce convective losses relative to radiative losses, whereas external receivers expose tubes to wind and sky, increasing forced convection and radiative exchange. In the convective pathway, ambient temperature, wind speed, and wind direction are primary drivers, while receiver orientation, inclination, and aperture ratio further modulate heat removal. Radiative losses depend on surface absorptivity and emissivity and on geometry through aperture design and view factors, with ambient temperature again exerting a strong influence.

Category 3: Mitigation strategies. This category targets loss reduction to raise overall effectiveness. Advanced materials, including aerogels, phase change materials, and high temperature absorber coatings, reduce both radiative and convective losses. Secondary flow control using air curtains can suppress natural convection in external and cavity receivers and, under low wind, also diminish forced convection. Geometry optimization, through alternative tube arrangements, innovative layouts, and added fins, reduces convective and radiative losses by reshaping flow patterns and view factors. Although finned designs are a subset of geometry optimization, their widespread use and integration with other measures justify treating them as a distinct class in comparative assessments.

As shown in Fig. 7, the set of parameters that can be addressed through analysis and mitigation of thermal losses is much larger than the limited group that defines thermal efficiency alone. Focusing on these loss-related parameters therefore offers a broader and more promising design space for improving CSP receiver efficiency and reliability.

6. Thermal losses of external receivers

6.1. Thermal loss analysis

6.1.1. External cylindrical receiver

Thermal loss in external cylindrical receivers is governed mainly by geometry, operating conditions, and optical design, with wind, temperature, and flux nonuniformity dominating their relative contributions. Christian and Ho [67] partitioned an external receiver into 24 panels and reported convective loss discrepancies of 4.9%, 4.4%, and 10.5% as external convection increased, establishing a benchmark and showing that predictive accuracy degrades as forced convection strengthens.

Operational control can partly compensate for geometric sensitivity. Emerick et al. [68] showed that increasing CO_2 mass flow rate reduces radiative loss and lowers sensitivity to geometric variations, so flow scheduling can recover efficiency otherwise lost to shape imperfections or nonuniform flux. Mass flow control thus complements aperture design and panelization as an adaptive lever under changing weather and flux.

Unsteady aerothermal effects challenge steady, axisymmetric models. Zhang et al. [69] showed that unsteadiness raises convective and radiative losses downstream as the tube wall temperature increases, while a Crescent Dunes analysis by Qaisrani et al. [70] found enhanced mixed convection and a shift of maximum heat transfer to a 115° stagnation point. Neglecting unsteadiness and wind direction therefore underpredicts spatial nonuniformity of temperature and losses, especially for receivers directly exposed to wind.

Cylindrical receivers start with lower and more uniform areal loss than cavities, but performance still hinges on the wind regime and flux distribution. Effective designs couple geometry and optical layout with active operating control, use validated panelized models, schedule CO_2 mass flow to mitigate sensitivity to geometric and flux nonuniformity, and account for unsteady wind to avoid downstream hot spots and loss escalation.

6.1.2. External flat receiver

Flat external receivers, which expose a single surface, are more sensitive to wind angle and speed than cylindrical receivers, which receive flux more uniformly and shed heat more symmetrically. Under controlled tests, Cagnoli et al. [30] reported convective losses rising from

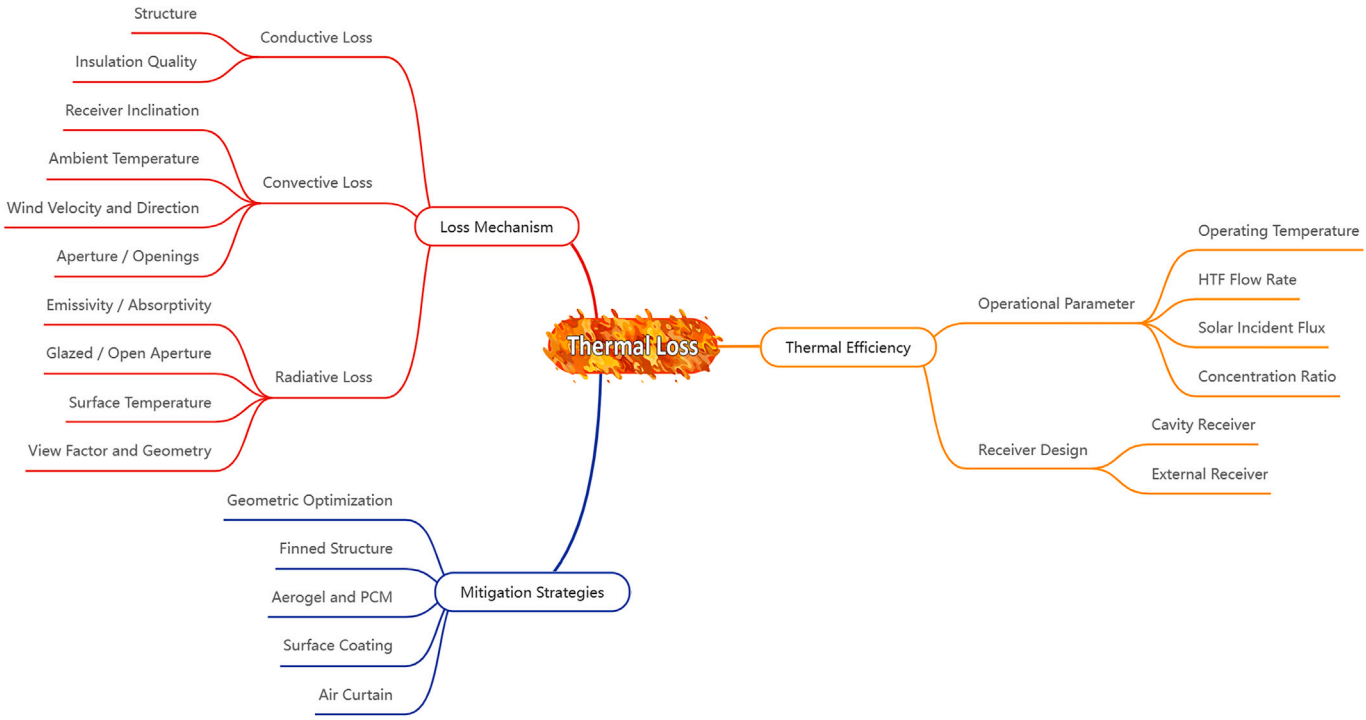


Fig. 7. Classification of thermal loss research.

10.9 kW at 0 m/s to 22.5 kW at 10 m/s (about 106%), with losses peaking for a 75° wind direction that generates inlet and outlet vortices. Consistently, Torres et al. [71] showed that mixed convection in a tilted cuboid receiver peaks near an 80° pitch, where forced convection contributes about 75% of total heat transfer. Orientation therefore amplifies wind influence even when buoyancy is present, and small changes in pitch or approach angle can shift the system into a forced-convection regime.

Mitigation for flat receivers emphasizes aerodynamic and geometric control at the aperture. Qaisrani et al. [72] found that losses are maximized when wind penetrates the opening and are reduced for head-on wind, while a 1 m wind-blocking wall cut losses by 33% at 9 m/s, underscoring the value of shielding and orientation. Thermally, Thirunavukkarasu and Cheralathan [73] observed that as the working fluid temperature increased from 30 °C to 100 °C, the overall thermal loss coefficient fell from about 440 to 182 W/m^2 (about 59%) under 380–750 W/m^2 irradiance, indicating a shift from convective to radiative dominance.

Internal heat-transfer enhancements can increase coolant-side heat transfer and, in many receiver designs, reduce absorber surface temperature non-uniformity by improving internal heat removal. Vishnu and Senthil [74] obtained thermal loss coefficients of 25.8–28.6 W/m^2·K using internally finned spiral absorbers. Vengadesan et al. [75] reported improved temperature distribution with square-tube fins and a reduction in average overall heat loss from 2.9 kW at 0.025 kg/s to 2.5 kW at 0.042 kg/s. Vishnu and Senthil [76] likewise observed that increasing coolant flow reduces both peak and average heat losses and decreases the overall heat loss coefficient. These trends suggest that lowering absorber surface temperature tends to reduce external losses (convective and radiative), although the dominant loss mode depends on wind/operating conditions, and any net benefit should be weighed against added pressure drop and pumping power.

Surface texturing and absorber form factor also influence the radiative–convective split at elevated temperatures. Lubkoll et al. [77] evaluated a spiky absorber for air preheating up to 800 °C and found radiative losses of 5.3% and convective losses of 9.5%, a total of 14.8% of incident flux in no wind. Radiative loss rose with nozzle diameter until stabilizing at 20 mm, indicating that geometric details governing view factor and internal recirculation can alter partitioning even in quiescent conditions.

By comparison, cylindrical absorbers tend to show lower absolute losses under similar winds. Thirunavukkarasu and Cheralathan [78] reported convective losses of 140–200 W and radiative losses of 85–110 W, totaling about 260 W. This contrasts with flat receivers at the kilowatt scale and highlights the need to normalize by aperture area, perimeter, irradiance, setpoint temperature, and wind regime. After normalization, flat receivers remain more sensitive to wind magnitude and approach angle and benefit most from shielding and orientation control, whereas cylindrical receivers benefit from geometric symmetry and show lower areal and perimeter-normalized losses under the same forcing.

Yang et al. [79] proposed a chloride salt receiver and found that as the flow rate increased from 6.32 to 14.04 L/min at inlet temperatures of 609.16 °C, 668.46 °C, and 723.24 °C, total thermal loss rose by 26.62%, 32.83%, and 40.92%. Over the same flow increase, radiative loss grew by 31.17%, 38.08%, and 45.63%, while convective loss increased by 19.99%, 25.29%, and 31.88%. Higher flow can therefore raise surface temperature and radiative emission even while evening gradients and limiting some convective peaks, so the net effect depends on operating temperature and the radiative fraction.

Overall, the evidence suggests a practical hierarchy for flat receivers. Shielding and orientation should first limit wind access; internal fins and higher mass flow then reduce wall temperature and smooth gradients; and aperture and surface details finally tune the radiative–convective split at high temperature. When comparisons are normalized by geometry and exposure, cylindrical receivers retain a lower baseline loss due to symmetric shedding and more uniform flux, while flat receivers require stronger aerodynamic management.

For external receivers, as shown in Fig. 8, key parameters governing total thermal loss are wind regime, orientation, shielding, operating temperature, mass flow, geometry and aperture, internal enhancements, and surface properties. Wind velocity and approach angle are primary drivers of convection, with flat plates being especially sensitive and with

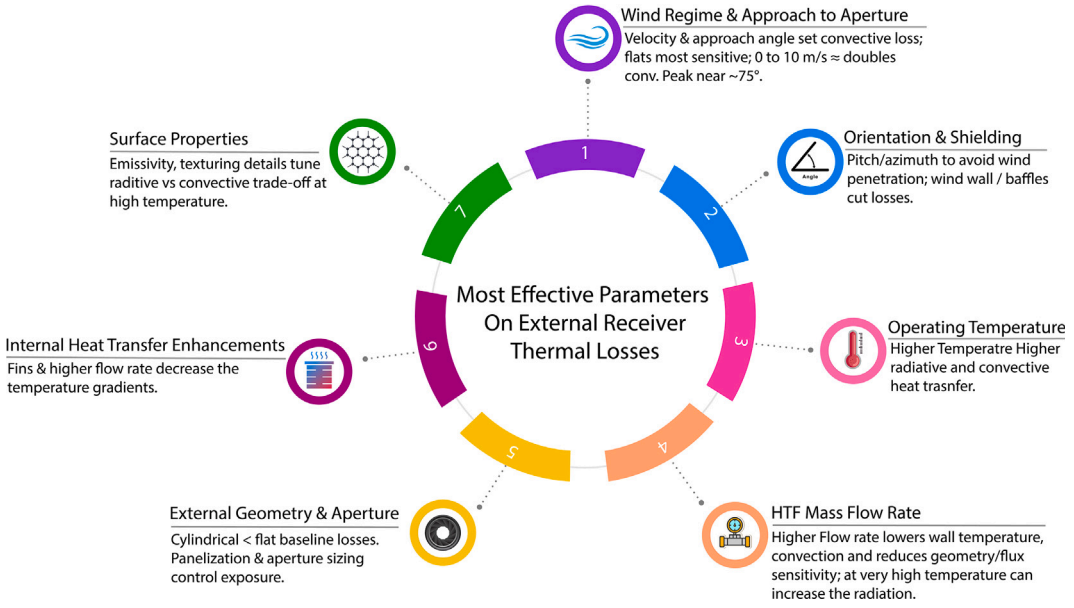


Fig. 8. Most effective parameters governing thermal loss in external receivers (vectors from [80,81]).

losses that can roughly double over practical wind ranges. Orientation and simple shields or walls that block direct ingress help keep convection low by limiting penetration at the opening. Operating temperature shifts the balance toward radiation because of the fourth-power dependence, while the effective temperature difference that drives convection can decrease as working temperature rises. Increasing HTF mass flow reduces wall temperature and gradients, lowering convective loss and reducing sensitivity to geometric and flux nonuniformity, although at very high temperatures or with certain fluids radiative transfer can increase. Geometry and aperture set baseline exposure, with cylindrical layouts shedding heat more symmetrically and exhibiting lower normalized losses than flat plates when exposure is matched. Internal features such as fins or spiral absorbers, together with higher coolant flow, even out the temperature field and reduce convective pathways, provided pumping penalties are acceptable. Finally, surface emissivity, texturing, and view factor-related details tune the partition between radiation and convection at high temperatures and can significantly reduce emission without causing large changes to the flow field.

6.2. Thermal loss mitigation

6.2.1. External cylindrical receiver

Thermal loss mitigation in cylindrical and semi-cylindrical external receivers relies on coordinated changes to geometry, surfaces, and materials, with the most effective choices varying with temperature and wind (Fig. 9). Ho et al. [29] combined microscale coatings, mesoscale tube geometry, and macroscale layout and reported up to a 50% reduction in total thermal loss at 800 °C. Although fins increased local convective and radiative flux because of the larger area, net loss still fell, especially when solar absorptance was modest, showing that appropriate surface properties can offset area penalties from geometric add-ons.

Schmitt et al. [85] achieved a total thermal loss reduction of 1.92 MW, comprising 1.32 MW radiative and 0.60 MW convective, by installing a dome roof covering 30% of the receiver at 6.5 m/s wind. The total reduction was 1.79 MW at 2.45 m/s and 0.60 MW at 12.3 m/s, indicating that shielding which reduces exposure to the cold sky is most effective at lower wind speeds, while higher wind weakens the benefit through increased convection.

Air management provides incremental relief under wind. Wang et al. [86] used a segmented air curtain on a Solar Two receiver and reported a 9.6% reduction in convective loss with only a small efficiency gain. In another study, Wang et al. [87] added blades, increasing efficiency by 3.8%, reducing total loss by 22%, and yielding a more uniform flux distribution than a conventional receiver; peak flux was 38.6% lower than in the conventional design. Modest geometric features and airflow control can thus suppress local peaks and smooth the flux field, although when radiative losses dominate the net efficiency gain is limited.

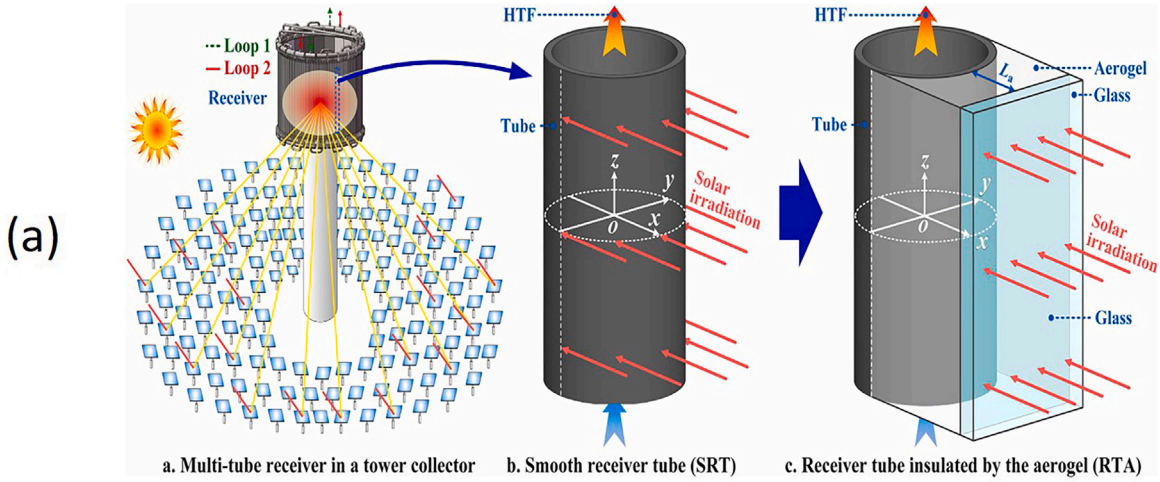
Surface and material strategies change the balance between radiative and reflective losses. Wang et al. [83] paired fins with nanostructured coatings that lower infrared emissivity and reabsorb reflected sunlight, keeping reflective and radiative losses below 5% of intercepted energy. Ye et al. [82] applied aerogel layers to absorber tubes and achieved large loss reductions as thickness increased; total loss decreased from 1357 W/m to −373 W/m at 15 mm aerogel, indicating heat flowing from the aerogel layer into the absorber, while optical efficiency declined from 95.15% to 86%, highlighting the need to balance thermal benefit against optical penalty.

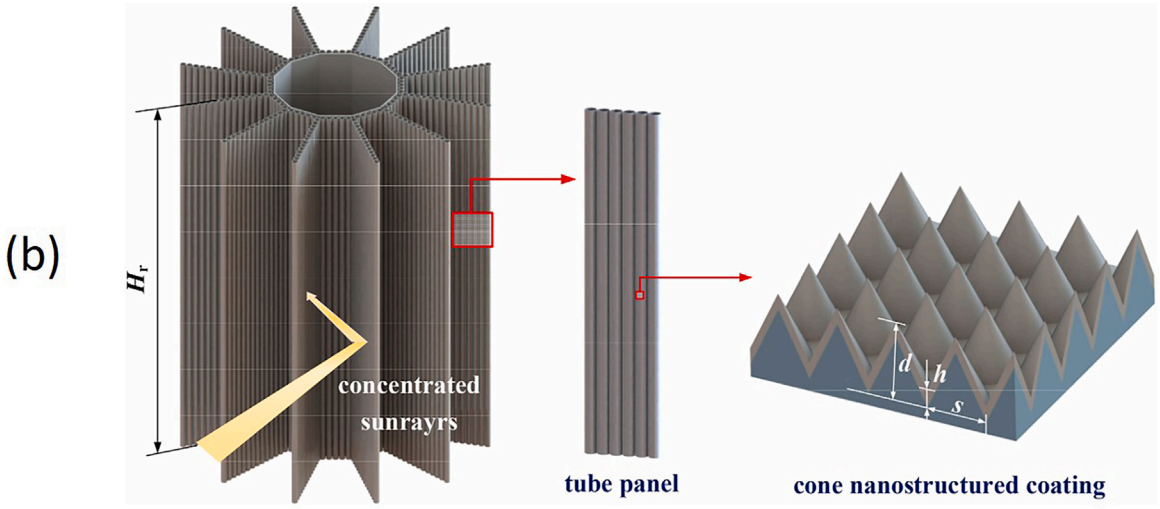
Panelization and internal flow pathways can lower radiative exchange without expanding exposed area. Montes et al. [84] proposed a microchannel absorber with two flow passages in a star-shaped receiver and showed that increasing panels from three to eight reduced radiative losses from 1290.33 kW to 684.12 kW by decreasing the external view factor. Partitioning the aperture and shaping the enclosure to limit sky view are therefore robust methods to reduce radiative exchange while maintaining flux control.

For receivers operated near 800 °C with modest solar absorptance, aerogel insulation delivers the largest absolute reductions in thermal loss (Fig. 10), with geometrical modifications that reduce view factor coming next. Because there is a trade-off between radiative and convective loss, particularly in geometric modifications where reducing one component can increase the other, prioritizing the dominant mechanism at the target operating point is most effective. Air curtains and related airflow controls mainly affect convection and thus contribute less when radiative loss dominates.

6.2.2. External flat receiver

For flat receivers, the most effective lever depends on whether the main constraint is aerodynamic, optical, or thermal. Under laboratory conditions, airflow management yields measurable but usually moderate





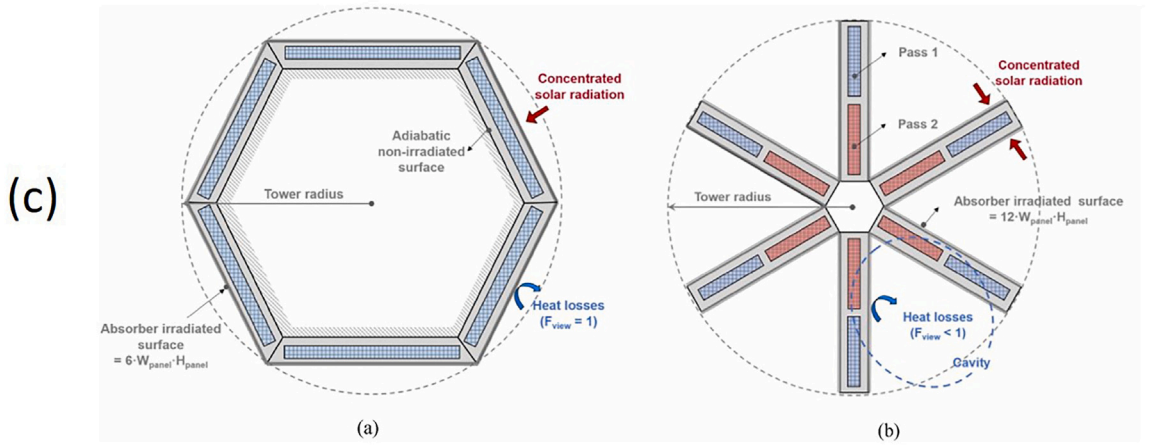


Fig. 9. Mitigation strategies for external receivers: (a) aerogel insulation [82], (b) bladed receiver with cone nanostructured coating [83], (c) microchannels in a star-shaped receiver [84]. (Obtained with permission from Wang et al. [83] and Ye et al. [82]).

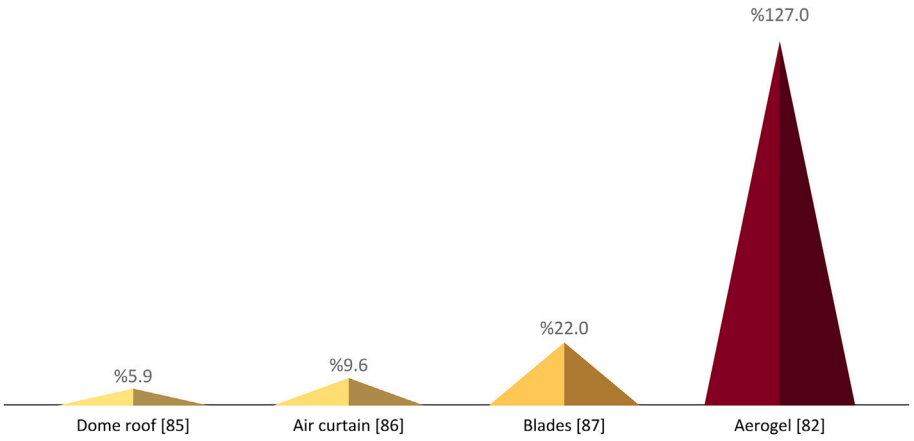


Fig. 10. Relative total thermal loss reduction achieved by different strategies applied to external receivers; dome roof [85], air curtain [86], blades [87], aerogel [82].

average gains. Mondal et al. [88] reported a 31.2% reduction in convective loss from a 110 °C flat plate using a 45° tilted air curtain at 2.5 m/s, and a follow-up study [89] achieved an 18.37% reduction with a 30 mm nozzle and 30 mm gap at 5.5 m/s. Air curtains are therefore most effective at suppressing peak convective events, while average savings remain smaller unless jet geometry and nozzle–gap spacing are tuned to the site wind field.

Geometric refinement reshapes the aperture and internal passages to trade added surface area for reduced view factor and improved light trapping, provided flow choking is avoided. Bladed and aperture-controlled concepts by Wang and Pye [90] increased efficiency by 9.2% at 845 kW/m^2, and later optimization by Wang et al. [91] using 15 blades, a 4.5 m blade depth, and a 63.9° blade angle improved optical performance. Complementary flow–heat transfer studies define the operating envelope. Ghanadi et al. [92] showed that although higher wall temperature and bulk velocity elevate convection, extending blade length sixfold can reduce convective losses by up to 75%, and increasing pitch from 26° to 70° cuts convection by about 40%. In contrast, Torres et al. [93] found a maximum heat transfer coefficient at a 45° tilt, attributed to optimal vorticity, with greater tilt lowering efficiency, and observed that additional blades can obstruct flow and reduce performance. Geometry is thus most effective when it reduces the view factor and flattens peak flux without inducing recirculation or excessive pressure drop. Thermal control strategies, including phase change materials (PCMs), internal fins, and enhanced coolant circulation, target the internal temperature field and the radiative–convective split rather than external aerodynamics. For flat receivers on parabolic dishes, Senthil [94] showed that a KNO_3–$NaNO_3$ PCM with vertical fins reduced thermal loss by 1.7% relative to horizontal fins across 0.5–2.2 m/s winds. Nallaperumal et al. [95] found that vertical fins lowered total losses from 5513.8 W to 4616.3 W at higher HTF flow (about 16.3%), while cross fins reduced losses further to 4284.6–3183.4 W as flow increased from 0.056 to 0.111 kg/s, about 7–31% below the vertical fin case and 22–42% below the baseline. Added surface area can therefore provide a net benefit when it decreases the effective view factor, supports higher coolant throughput, and preserves acceptable pumping power.

Overall, airflow management such as tilted air curtains reduces wind-driven convection but yields moderate average savings unless tuned to local winds. Geometric refinement offers the greatest potential when it lowers the aperture view factor and avoids recirculation or excessive pressure drop; increasing blade length or pitch can markedly cut convective losses, whereas excessive tilt or overblading can raise heat transfer and hinder performance. Thermal measures, including PCMs, fins, and surface shaping, provide smaller but reliable gains by smoothing the temperature field and permitting higher coolant flow without prohibitive pumping power. The best strategy is to match interventions to the dominant loss mechanism at the intended operating point: first optimize geometry to minimize the view factor while preserving healthy flow, then apply materials and fins to stabilize temperatures and support throughput, and finally tune airflow controls to local winds to suppress residual convective peaks.

7. Thermal losses of cavity receivers

Beyond external receivers, cavity receivers are a major class of concentrating absorbers. Their recessed geometry and controlled aperture reduce thermal losses and support higher operating temperatures. As summarized in Table 3, recent work has focused on quantifying and mitigating thermal losses across receiver types as a central determinant of efficiency [96–100].

Studies are commonly organized by geometry into four main types, cylindrical, hemispherical, conical, and tower-specific designs, with less common hyperbolic [101] and combined cylindrical–spherical concepts [102]. Mitigation methods are often grouped using the same scheme, clarifying how aperture control, view factor, and internal recirculation translate into lower convective and radiative losses at similar setpoints.

7.1. Thermal loss analysis

7.1.1. Cylindrical cavity receiver

Flesch et al. [103,104] reported that wind has little effect on large horizontal cavities, whereas inclining the receiver so that the aperture faces the wind substantially increases wind-driven convection; alignments that limit direct ingress keep convective penalties small.

Wind and temperature interact to set the loss regime. Shen et al. [105] showed that higher surface temperatures increase total losses, while wind can first reduce losses relative to no wind and then increase them as speed rises. Xiao et al. [106] found that dish concentrators generally mitigate convection except when wind approaches the convex side at low tilts from 0° to 17°. From 0° to 30°, convective losses first decrease with wind speed and then rise, whereas from 60° to 90° the increase with speed is nearly linear. Wu et al. [107] experimentally confirmed wind speed as the dominant driver, with peak mixed convection losses at 75°–90° inclination. Tilt and approach direction therefore define the operating regime and the same wind speed can have opposite effects depending on orientation.

Geometry and operating conditions jointly determine both the magnitude of receiver losses and how they partition among convection and radiation. Lee et al. [108] showed that, at wind speeds below 3 m/s, increasing the aperture ratio from 0.33 to 0.75 can change total losses by up to 75%; however, this sensitivity largely disappears above 4 m/s, indicating that geometry is most influential in light winds, whereas

aerodynamics dominate under stronger winds. Yazdanipour et al. [109] reported strong tilt dependence of convection, with convective losses peaking at −30° where they account for 63% of total loss and decreasing to 19% at +90°, while radiative losses vary less with tilt. Consistent with this inclination-dominated behavior, Wu et al. [110] found that increasing inclination can reduce convective losses of a rotating cylindrical receiver by up to 80% (up to 90% for downward-facing cases), whereas rotation has a much smaller effect, altering convective losses by at most about ±10% in their tested range. Zou et al. [111] similarly observed that enlarging the aperture diameter from 184 mm to 300 mm and adding tube loops substantially increases total loss, consistent with enhanced exchange through a larger opening and increased exposed area. For prediction across practical geometries, Abbasi Shavazi et al. [112] proposed a Nusselt-number correlation for natural convection over Grashof numbers from 2.6×10^5 to 1.4×10^7 that accounts for nonuniform surface temperature and aspect ratio.

Wind management features can shift performance. Swanepoel et al. [113] examined wind-skirted receivers in solar dish Brayton cycles and found up to a 61% increase in thermal loss at a 22.5° elevation compared with 90°, indicating that skirts can worsen losses when they steer flow unfavorably at intermediate tilts. In contrast, Bashir and Ali [114] compared cylindrical cavities with U-shaped, conical, and helical tube layouts and reported an exponential reduction in thermal loss from about 600 W at 0° to roughly 20 W at 90° inclination, showing how internal flow paths and upright orientation can suppress convection.

Zhi et al. [115] analyzed a cylindrical receiver and found that in a downward-facing position, a larger stagnation zone forms in the cavity, which limits air escape and reduces convective loss. They also reported that when the ambient temperature increases, the surface-to-ambient temperature difference decreases and convective loss is reduced.

Overall, wind regime, tilt, and aperture exposure jointly govern losses. Horizontal or well-shielded orientations limit wind access, low tilts can show nonmonotonic wind responses, and larger apertures or unfavorable skirts amplify convection. Internal layouts and dish geometry can suppress convection when they discourage through flow, while higher ambient temperature reduces convective driving by narrowing temperature differences. A practical sequence is to use tilt and shielding to limit convective access, choose aperture and internals that preserve optical capture without opening direct flow paths, and tune operation with temperature and wind to maintain a favorable balance between convection and radiation.

7.1.2. Hemispherical cavity receiver

Hemispherical cavity receivers are of interest because their geometry and thermal behavior differ from other types. As summarized in Table 3, total thermal loss depends on inclination, operating temperature, aperture configuration, insulation, and wind. Inclination is the dominant control because it sets the relative strengths of natural and forced convection and thus the convective–radiative split. Reddy et al. [147] reported that under side-on wind at 5 m/s, convective losses can be seven to eight times greater than those in natural convection. Li et al. [148] showed that rotating the aperture from vertical, 0°, to horizontal, 90°, markedly lowers natural convective loss, which is attributed to a stagnation air layer and improved alignment between velocity and temperature gradients.

Vikram and Reddy [149] confirmed maximum convective loss at 0° and minimum at 90°, while radiative loss remains nearly unchanged. Construction choices set the baseline; a larger diameter ratio and higher cavity cover emissivity increase total loss, whereas thicker insulation reduces it. Under outdoor conditions, wind direction modulates the inclination effect. Reddy et al. [150] found that with side-on wind, increasing inclination consistently reduces loss, whereas with head-on wind the loss first increases from 0° to 30°, then decreases from 30° to 75°, and rises again near 90°, with these variations intensifying as wind speed increases. Using numerical modeling over wind directions −90° to +90°, speeds 0–10 m/s, and tilts 0°–90°, Reddy et al. [151] further showed that as the surface tilts from horizontal to vertical, the contribution of natural convection decreases, so wind increasingly dominates at higher tilts. Isolating wind speed, Loni et al. [152] reported total loss from about 112 W to 333 W between 0.6 and 4.3 m/s, with conduction contributing less than 10% of mixed convective loss. Shewale et al. [153], combining experiments and simulations at 150 °C, 225 °C, and 300 °C and tilts 0°–90°, found that convection diminishes with tilt. Under wind, losses are largest for head-on flow at 0°, whereas a 0° side-on wind produces less convective loss than even the no-wind baseline.

Aperture geometry couples with inclination to set exposure and recirculation. Tan et al. [154] reported maximum losses at a 0.15 m aperture with 0° inclination and minimum losses at a 0.25 m aperture with 90° tilt, showing that aperture size and tilt act in combination. In experiments spanning aperture ratios 0.46–0.93, glazing thicknesses 2–6 mm, and surface temperatures 90–180 °C, Bopche and Kumar [155] observed a peak efficiency of 79.05% at an aperture ratio of 0.6 and identified 4 mm glass as optimal. Natural convection accounts for about 28.6% at 90°, 42.9% at 60°, 48.9% at 45°, and 53.45% at 30°, indicating a larger buoyancy contribution as tilt decreases.

Extending the design space, Khan et al. [156] proposed a hemi-ellipsoidal receiver and evaluated its thermal and optical performance. At higher eccentricity this geometry achieves better thermal performance and lower thermal loss than comparison shapes, attributed to secondary vorticity inside the cavity that reduces air velocities and convective exchange.

In overview, inclination is the primary lever for hemispherical-type receivers: moving from 0° to 90° reduces convection while leaving radiation nearly unchanged. Aperture size should then be coordinated with tilt to preserve optical capture without promoting through flow; larger apertures at low tilt increase losses, whereas larger apertures at upright tilt can be acceptable. Materials and insulation set the baseline, and site wind should be managed by minimizing head-on exposure at low inclinations. Hemi-ellipsoidal forms can further suppress convection when optical requirements allow.

7.1.3. Conical cavity receiver

Conical cavity absorbers have been examined extensively to understand how aerodynamic conditions and geometric design interact. Wind speed, wind orientation, cone angle, aperture size, and cavity dimensions jointly set the balance between convective and radiative loss, and the surrounding reflector or dish reshapes the external flow. Uzair et al. [157] showed that for winds of 1–5 m/s, when the approach angle exceeds 30° from the dish axis, convective losses can fall below natural-convection levels, and at 10–20 m/s similar approach angles continue to mitigate convection. Building on this, Uzair et al. [158] found that introducing a dish can reduce total losses by up to 40%.

Cone angle and aperture choice alter view factor and internal circulation. Zhang et al. [159] reported two patterns, in one, as cone angle increased 0°–20°, radiative loss rose from 2370 W to 2773 W, while convection first decreased to about 1684 W and then increased; in the other, convection fell from 1945 W to 1566 W, while radiation decreased from 3377 W to 2304 W. For beam-down configurations, Li et al. [160] swept cone angles 52°–140° and observed efficiencies of 39% at $\Delta T = 181$ K and 60% at $\Delta T = 81$ K, with a minimum total loss near a 100° cone. Geometry effects were further quantified by Venkatachalam et al. [161], who tested aspect ratios of 0.8, 1.0, and 1.2 and reported average efficiencies of 57.39%, 44.06%, and 45.87% with corresponding overall loss factors of 58, 100, and 84 W/K, indicating that the most compact absorber, AR 0.8, maximizes efficiency and minimizes losses.

Material and thermal design can amplify or offset geometric effects. Bashir et al. [162] studied receivers with PCM and found that enlarging the aperture from 0.18 m to 0.30 m keeps convection near 1 kW but increases radiation from just over 4 kW to nearly 14 kW. Raising surface temperature from 1000 K to 1550 K produces only a small increase in convection, while radiation grows sharply. Increasing cavity size also raises total loss; for a 0.21 m aperture and 0.30 m cavity length, the

Table 3
Previous studies involving heat losses of cavity receivers (Note: Num = Numerical, Exp = Experimental, Anal = Analytical, Temp (temp) = Temperature).

Ref.	Topic	Methods	Evaluated Factors	Thermal Performance	Heat Loss	Remark
[116]	Aspect ratio	Num	L/D 0.5–3; Wind 0–14 m/s	Eff. 84–89% (0 m/s), 80–87% (14 m/s)	Conv. 35–45 W at 400 °C, min at 2 m/s	Best at L/D = 3
[117]	Wind, yaw	Exp	Yaw 0–90°; Wind 0–12 m/s	–	Conv. < 0.5 to < 2 kW (0–12 m/s) at 45° yaw; Total loss ~1.5 to < 0.5 kW at 6 m/s (yaw 0–90°)	Front section dominates at low wind
[118]	Forced convection	Exp	Tilt 0, 30, 60°; Aper. 0.6–1.0; Wind angle 0–180°; Re 2×10^6–8×10^6	–	Max Nu at 30°, Aper. 0.8–1.0; Higher Re increases conv.	Peak at wind 60–80°
[119]	Rectangular cavity	Num	Tilt 0–90°; Emiss. 0.2–1.0; Aspect 1–2	–	Total ~600–750 W (tilt 0–90°); Rad. ~400–1500 W (emiss. 0.2–1.0); Conv. ↓~30% with higher aspect	Higher wall Temp increases loss
[120]	Tilt, wind	Num, Exp	Tilt 0–90°; Wind 0.5–4 m/s	Eff. 40–50%	Rad. ~30% of total; Wind ↑ → conv. ↑	Min loss at 0° (low wind) shifting to 22.5° (higher wind)
[121]	Stirling cavity	Exp	Aper. 0.5–1.0; H/D 0.53–1.46	–	Conv. 0–10 W (300–600 K); Smaller aper. reduces loss; Loss ↑ with Temp	Aper. ratio > position
[122]	Heat flux, tilt	Exp	Tilt 0–90°; Flux 250–1100 W/m^2	–	Conv. slightly ↑ with flux, strongly ↓ from 0° to 45°; Rad. mainly set by flux	–
[123]	Wind, tilt, direction	Num	Wind 2–10 m/s; Tilt 0–90°; Incidence −90°–90°	–	Mixed conv. < natural at low wind, > at high; Tilt effect weakens with wind	–
[124]	Wall Temp, tilt	Exp	Wind 0–9 m/s; Yaw 0–90°; Tilt 15–90°	–	Wall Temp shifts loss up to 50%, to 20% head on; Downward tilts ~3× higher; Beam up minimal	–
[125]	Temp, tilt, aperture	Num	Tilt 0 to −90°; Temp 650–1150 K; Aper. 0.5–1	–	Natural conv. ↑ with Temp and Aper.; Peak near −30°; Lower Aper. weakens Temp effect	–
[126]	Inclination	Exp	L/D 1, 2; Tilt 0–90°	–	Rad. >30 W to <85 W with tilt	–
[127]	Receiver–Stirling	Num	Temp 700–1000 K; Tilt 0–90°; Aper. 0.25–1	Eff. +8.8% (21.34→30.11%)	At 0°: total ~1000→6000 W (700→1000 K); At 900 K: total ~4000→3500 W (0→90°); At 0° rad. 74–81%	Higher Temp boosts conv. and rad.; Smaller Aper. lowers losses
[128]	Radiative loss model	Num	Temp 373–2273 K; Emiss. 0.2–0.8; L/D 0.75–4.5	–	Rad. 0.018 kW→41 kW (Temp); 2.7→4.4 kW (emiss.); 3.9→4.1 kW (L/D)	–
[129]	CFD code compare	Num	Tilt 0–90°	–	Versus exp.: conv. under by ~45% (const Temp), ~32% (const flux); Total under by 21%, rad. over by 26%	–
[130]	Photothermal, MCRT	Num	Focus, receiver offset ±0.06; Rim 30–60°; Absorpt. 0.4–1; $\dot{m}$ 0.01–0.1 kg/s	At 1000 W/m^2: Eff. < 95%*to* > 90% with offset; ~ 94% →~99% with $\dot{m}$ 0.01→0.05	Losses ↑ with offset, rim, absorpt.; Rad. more sensitive to offset; Conv. dominates at higher rim	–
[131]	Hybrid combustor	Num	L/D 3, 5, 7; HTF tubes 1 vs 2 rows	Solar only Eff. 79.7, 82, 82%; 2 rows 95→ ~97%	Wall 2.7, 3.07, 3.9 kW; 1 row higher conv., rad.	1 row higher losses
[132]	20 kWh hybrid	Exp	Modes: solar, comb., mixed; Input 0.8 kW, 10.8 kW	–	Solar loss 0.3033 kW; Mixed 3.04–3.53 kW; Conv. ~60% of total	–
[133]	Geometry effects	Num	Aper. 0.184–0.3 m; Cavity dia. 0.35–0.7 m	Eff. 71→67% (cavity dia. 0.35→0.7 m)	Rad. 2989→7754 W (aper. ↑)	Conv. nearly triples with larger cavity
[134]	L/D, Temp	Exp, Anal	L/D 0.25–7.5; Temp 600–1200°C	Eff. ↑ with Temp, ↓ with L/D	Conv. peaks at L/D = 2; Temp effect small for L/D<1	–
[135]	DNI, inlet Temp, flow	Exp	DNI 201.7–504.3 W/m^2; Inlet 100–250°C; $\dot{m}$ 0.05–0.11 kg/s	Eff. 69.80→66.02% (DNI); 67.9→61.4% (inlet); 66.0→67.6% ($\dot{m}$)	With DNI: Conv. 407.1–1087.4 W, Rad. 284.5–412.1 W; Inlet: Conv. 916.5–965.7 W, Rad. 349.1–367.7 W; $\dot{m}$: Conv. 934.4–889.9 W, Rad. 364.1–329.3 W, Other 721.1–708.9 W	–
[136]	Iris vs rotary aperture	Exp	Mechanism	–	Loss ↑ with absorpt., ↓ with reflect.; Iris up to 1.2% higher; Re radiative ~11–12% of emissive	Similar trends for both
[137]	In situ steam receiver (> 3 bar)	Exp	–	Receiver Eff. 50%; Collector Eff. 42%	Avg. loss 865 W; Nu: Top/Bottom ~78, Left/Right 89	–
[138]	Analytical model, solar–Stirling	Anal	–	–	Daylight avg.: Conv. <500 W; Rad. >550 W	–
[139]	Redox reactor optimization	Num, Exp	–	–	Loss 1087.55 to 539.4 kJ/kg	–
[140]	Helical tubes	Num	H/D 1–2; DNI 650, 1000 W/m^2; $\dot{m}$ 0.005–0.05 kg/s; Wind 0–12 m/s	Eff. >97→ >95% (H/D 1–2); ~95→ ~99% with $\dot{m}$	At 1000 W/m^2: < 90 → < 165 W (H/D 1–2); 650 W/m^2: < 60 → > 105 W; Higher $\dot{m}$ lowers loss	Wind: side on highest, head on lowest
[141]	Directly illuminated cavity	Num, Exp	Wind 0–10 m/s	–	At 1108 K: Refl. 2.2 kW, Emitted 1.3 kW, Conv. 0.98 kW; Total ~3.25→ ~4.25 kW	–
[142]	DNI effects	Num	DNI 400–800 W/m^2	Eff. −2.18% (184 mm aper.), −2.45% (280 mm)	Rad. share 70.1→74.6%	–
[143]	Wind, inclination	Num	Wind 0–15 m/s (back, side, front); Tilt 0 to −90°	–	With wind: Rad. ↓, Conv. ↑; Tilt effects depend on wind	–
[144]	Geometry compare	Exp	Configs: conventional, extended, extended + helical	Eff. 57.71, 60.93, 68.03%	Max 2.75, 2.63, 2.43 kW; Avg. 2.44, 2.20, 1.76 kW	–
[145]	Air heated, splitter	Exp, Num	Air 1–5 m^3/h	–	Total ↑ as air ↓; Reflection ~2.94%; Cylinder outer: Rad. 14.78–29.89%, Conv. 18.11–28.57%; Glass: Rad. 4.64–10.52%, Conv. 2.41–3.75%; Inner surface rad. 4.27–9.83%	Down flow 11–48 W lower than up flow
[146]	Nanofluids	Exp	–	Eff. Al_2O_3/oil 59.13–62.15%, SiO_2/oil 56.89–58.55%, Thermal oil 57.71–58.85%	Loss coeff.: 346.38 (Al_2O_3/oil), 411.49 (SiO_2/oil), 419.84 (oil)	–

cavity contributed 7.2 kW alone and 18 kW when the front aperture was included. In complementary simulations, Bashir et al. [163] showed that with PCM-integrated receivers, convective loss exceeds 600 W at 0°, drops to ∼ 30 W at intermediate tilts, and remains below 50 W at 90°, and that optimum PCM configuration depends on tube layout. Surface treatment also matters. Sagade et al. [164] reported that using a selective coating raised efficiency from 48%, uncoated, to 63%, coated, for winds of 2.7–5.73 m/s, with small convective changes, forced coefficient about 3%, and natural convection about 0.32%.

For conical absorbers, priorities are to manage external aerodynamics through dish geometry and wind orientation, since shielding can reduce convection even at 10–20 m/s and cut total losses by up to 40%; select cone angle and aperture to control view factors and recirculation; tune scale and aspect ratio, with compact designs such as AR 0.8 offering higher efficiency and lower loss factors; and specify materials and PCM in concert with inclination, since PCM and coatings strongly affect radiative and convective losses at given tilts.

7.1.4. Tower-mounted cavity receivers

Tower-mounted cavity receivers differ from dish systems in exposure and geometry. Polyhedral faces form the cavity and flux arrives from a large heliostat field rather than a single dish, enabling large plants but often with higher absolute heat loss [165]. Flow direction relative to the aperture is the primary driver. Tu et al. [166] introduced a depth stretch, an added side wall, from 0 m to 3 m and achieved efficiencies of 82.5%–84.4%, while total losses fell from more than 940 kW to about 860 kW; an optimum stretch of 2 m balanced view factor benefits against added surface loss. Using a trapezoidal cross section, Hu et al. [167] showed that side-on wind minimizes loss, while perpendicular wind produces natural and mixed convection regimes depending on speed and inclination. Deng et al. [168] examined ambient temperature from −5 °C to 35 °C and width–depth ratios of 0.2–1, and found efficiency rising from about 80% to more than 81% as ambient temperature increased, with total losses declining; minimum fractional losses were about 15% radiative, 7% convective, and 22% total, with an optimal width–depth ratio near 0.5. Slootweg et al. [169] increased HTF inlet velocity from 0–8 m/s in hexagonal pyramid elements and observed outlet temperature falling from more than 565 °C to more than 290 °C, while the thermal loss fraction decreased from more than 50% to less than 5% of incident power.

Optical and surface properties govern radiation, while coolant management stabilizes convection. Fang et al. [170] showed that an ideal selective coating behaves like a blackbody for solar absorption while minimizing reflective losses and that radiative loss is very sensitive to emissivity and temperature, whereas active cooling holds convection nearly constant. Tu et al. [171] found that moving the superheater within the cavity changes local convective and radiative distributions without changing total loss. Zhang et al. [172] identified an optimum cavity height where a lower inner surface temperature reduces radiation, but changes in convective area offset the gain. Tu et al. [173] varied wall emissivity 0.1–0.9 and reported efficiencies of 77%–80.7%, with total losses decreasing from more than 1350 kW to about 1150 kW as emissivity decreased; convective losses moved from more than 650 kW to about 600 kW, radiative losses fell from more than 350 kW to about 200 kW, and reflected power remained near 350 kW, leading to the conclusion that cavity wall emissivity exerts a larger influence than tube emissivity.

Panelization and aperture fraction set the baseline. Linares et al. [174] compared receiver configurations and found substantial radiative losses, both solar and infrared, while convective losses vary with panel-induced flow paths. Kim et al. [13] provided correlations linking wind velocity, aperture size, and surface temperature to radiative and convective losses, and noted cases where full cavities with small apertures become convection dominated.

At plant scale, Ortiz et al. [175] simulated a 2 MW tower and showed that moving from natural to mixed convection increased convective loss from 15.2 kW/m^2 to 23.9 kW/m^2, with radiative loss changing from 101.6 kW/m^2 to 106.1 kW/m^2. For a 1 MW molten salt receiver, Chang et al. [176] reported efficiencies of 75.14%–76.13%, with total loss increasing with tube temperature and mixed convection governed jointly by temperature, wind, and structure. Luo et al. [177] compared external and cavity towers and found a maximum system efficiency of 86.55%, with radiative and natural convective losses of 1378.8 kW and 701 kW, respectively; the external receiver exhibited higher convective and radiative losses due to hotter walls.

Thus, tower-mounted cavities respond to the same levers as conical cavities but with different sensitivities. Aperture fraction and cavity shape set the radiative view factor and internal recirculation; wind speed and approach direction decide whether convection is mitigated or amplified; and surface properties and active cooling tune contributions without changing total loss unless temperature or exposure decreases. Priorities are to set aperture and depth to minimize the view factor at the target flux, align the heliostat field and approach orientation to disrupt direct wind ingress, select coatings that lower emissivity at operating temperature, and schedule coolant flow more aggressively as scale and temperature increase.

7.1.5. Cavity receivers with other geometries

Besides efficiency, thermal loss is a critical criterion when proposing new receiver geometries. Singh et al. [178] showed that adding a leading edge to a liquid volumetric plated receiver slightly lowers system efficiency, from 91.75% to 90.76%, because the edge introduces additional reflection and thermal loss; with the edge, total losses reach 159.88 W, including 89.48 W thermal and 36.6 W additional reflection, whereas removing the edge yields 82.54 W total. For hyperbolic cavities, Mandal et al. [101] varied emissivity 0.2–1 and tilt 0°–90° and found that convective loss increases as the surface approaches horizontal, while radiative loss is essentially insensitive to tilt. At the component–system interface, Martinek et al. [179] proposed a cylindrical cavity receiver with hydrogen as the HTF that absorbs solar radiation on part of its lateral face. At a 4 kW input, they attributed about 9.5% of loss to reflection, 59% to thermal emission, and 11% to window conduction.

To sum up, as depicted in Fig. 11, the key parameters governing heat losses in cavity receivers are wind regime and approach to the aperture, which govern convective ingress; inclination or tilt, which determines the natural, mixed, or forced regime; aperture exposure in size and orientation, which increases convective access and radiative view factor as it enlarges; surroundings and flow management, including dishes, baffles, skirts, and nearby structures, which can block through flow or funnel wind; wall temperature and emissivity, which primarily control radiative loss; and cavity geometry and internals, including aspect ratio, cone angle, scale, and layout, which influence stagnation and recirculation. Compact forms and layouts that discourage through flow reduce convective loss, while scale and view factors shift the balance between convection and radiation.

7.2. Convective thermal loss correlations

Fig. 12 compares maximum-Nu envelopes obtained from published natural-convection correlations, plotted as Nu versus Ra. For each correlation, auxiliary variables were selected within the ranges reported in the original study to maximize Nu, and Ra was then swept over the correlation's stated validity range. The parameter ranges and the values used for each curve are tabulated in Appendix A. In general, hemispherical cavities show higher natural convective losses than cylindrical ones, except in the correlation of Jilte et al. [96], which yields higher values because it uses a larger surface-to-ambient temperature ratio. The correlations of Yazdanipour et al. [109] also show a strong orientation effect, a side-facing cylindrical receiver loses less heat by natural convection than an upward-facing one. Orientation is not the only control; other parameters act with orientation and can be decisive. In Jilte et al. [96], even though the Rayleigh number is lower than in other cylindrical

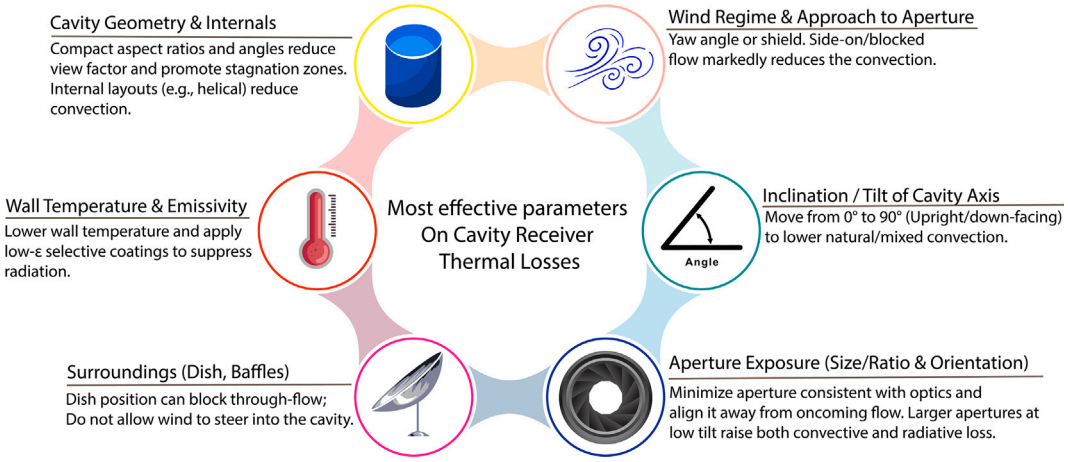


Fig. 11. Most effective parameters governing thermal loss in cavity receivers (vectors from [80,81]).

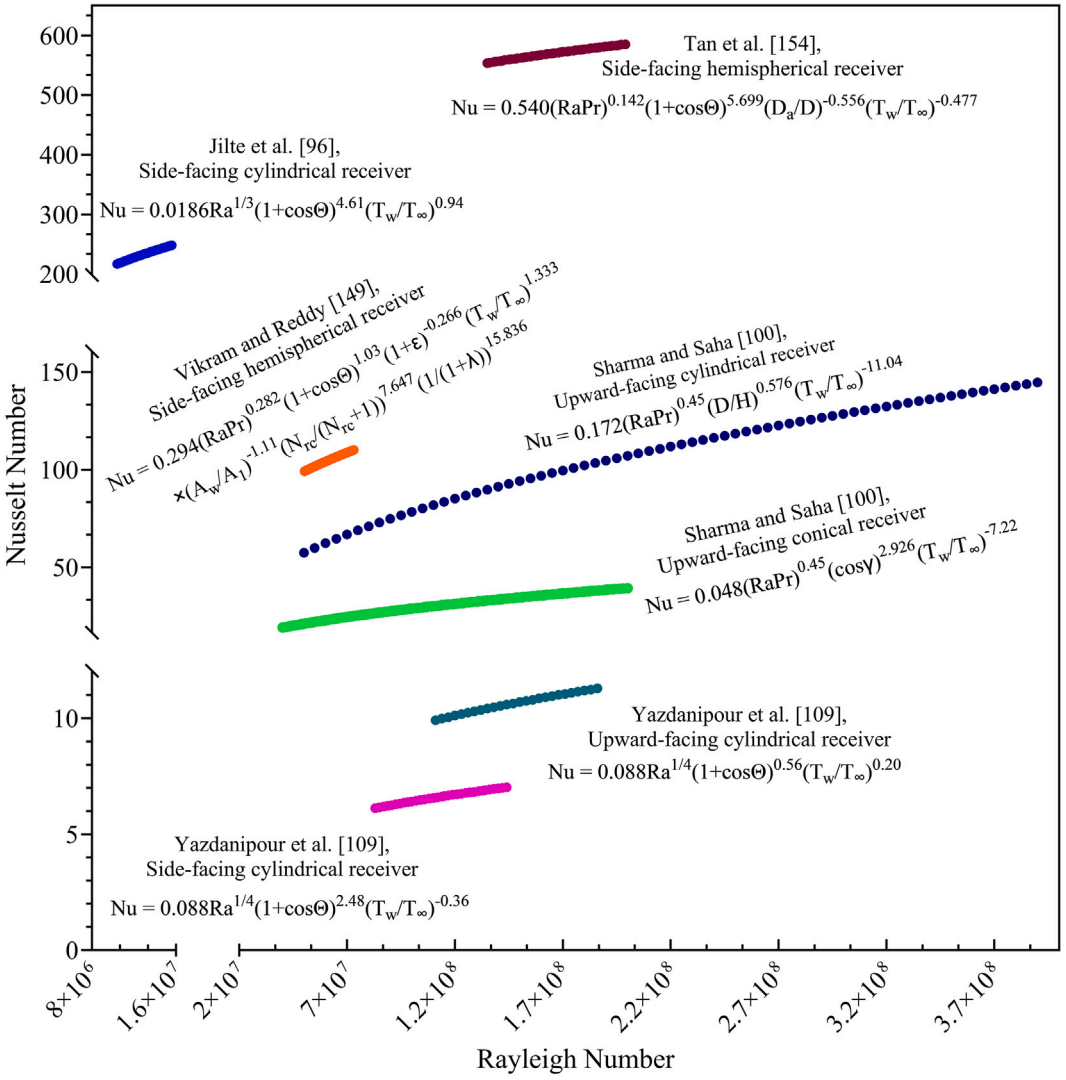


Fig. 12. Maximum-Nu envelopes from published Nusselt-number correlations for natural convective heat loss in cavity receivers. Each curve is generated by evaluating the corresponding literature correlation (as written on the figure) while sweeping Ra over the validity range reported in that source. For correlations that include additional variables (e.g., θ, T_w/T_∞, and geometry ratios), those variables were selected within the ranges stated by the original study to maximize Nu, so the plotted curves represent upper-bound predictions rather than a like-for-like comparison at identical boundary conditions across geometries. Ra: Rayleigh number; θ: orientation angle (°); T_w/T_∞: wall-to-ambient temperature ratio; D: diameter of receivers (m); D_a: aperture size (m); H: height (m); γ: half-cone angle (°); ε: emissivity; A_w/A_1: area ratio of receiver to aperture; N_{rc}: radiation–conduction number; λ: conductivity parameter.

cases and the receiver is side facing, the natural convection Nusselt number is the highest among the cylindrical receivers considered because the surface-to-ambient temperature ratio is larger. This aligns with other correlations in which coefficients and exponents on the surface-to-ambient temperature ratio exceed those on other variables, indicating its dominant influence on natural convective loss.

For hemispherical receivers, Tan et al. [154] predict much higher natural convection heat transfer than Vikram and Reddy [149]. A key reason is the larger inclination exponent in Tan et al., 5.699 versus 1.03 in Vikram and Reddy, and the higher sensitivity to the surface-to-ambient temperature ratio.

In the conical versus cylindrical comparison by Sharma and Saha [100], the conical receiver shows lower natural convection loss than the cylindrical receiver. One likely reason is that the surface-to-ambient temperature ratio term is about 50% stronger in the cylindrical correlation than in the conical correlation. Because the study did not report the ratio explicitly, a value of 1.2 was used in both correlations based on the reported temperature ranges. Geometry contributes as well, for similar base radius and height, a cone usually has less lateral surface area than a cylinder, which reduces the contact area for convection.

Overall, these correlations show that natural convective loss in cavity receivers depends on several parameters in a nonlinear way, which complicates the analysis and mitigation.

7.3. Thermal loss mitigation

Because thermal losses strongly constrain cavity receiver performance, many studies propose practical mitigation strategies (Fig. 13), grouped into three classes, geometrical modifications, secondary flow control, and other innovations.

7.3.1. Geometrical modifications

Geometrical changes target radiative and convective losses, most often via internal fins or aperture treatments. Across studies, fins mainly suppress natural convection, while glazing suppresses both convection and radiation, with a stronger influence on convection.

Mobasheri Shiri et al. [184] compared simple and finned downward-facing receivers and showed that fins reduced the convective share of total applied heat from 21% to 11%. Ngo et al. [185] used plate fins and reported up to 20% reductions in convective losses, about 5% in radiative losses, a maximum 8.2% decrease in total loss, and a 2% efficiency gain. In follow-up work, Ngo et al. [186] established that fin height is the dominant factor and thickness is secondary, with the optimum depending on inclination; at 0° and 30° thinner fins performed better, yielding up to 20% convective loss reduction at 0°. Higher Rayleigh numbers increase convection, but greater fin height, larger tilt angles, and increased fin count offset this penalty.

Bopche et al. [187] installed conical copper fins in hemispherical cavities and found regime-dependent optima. Under medium heat flux, convection dominant, the largest pitch produced the greatest total loss reduction, 14.32%, while under high heat flux, radiation dominant, the smallest pitch was best, 11.02%, because tighter spacing increases fin–fin view factor interactions that curb radiation despite added convective area.

Uhlig et al. [188] showed that a transparent window at the aperture increased efficiency from 75% to 83% for small receivers by reducing convection and radiation. Xiao et al. [189] showed that a quartz window makes natural convective loss essentially tilt independent, contrasting 35.94% tilt sensitivity without glazing, and reduces it by up to 71.79%. Daabo et al. [190] compared glazing across geometries and reported total loss reductions of 37.97% for conical, 12.16% for spherical, and 11.72% for cylindrical receivers.

These results indicate that well-designed fins and aperture glazing yield consistent reductions in heat loss. When convection dominates, larger fin pitch and added fins reduce losses by limiting air escape; when radiation dominates at higher temperatures, smaller pitch and glazing are more beneficial. Reported gains include up to 20% lower convective loss from fins, 14.32% total loss reduction via optimized pitch, and up to 8.2% efficiency gains from aperture windows.

7.3.2. Secondary flow

Actively managing a secondary airstream at the aperture disrupts buoyant exchange and can outperform passive geometry when convection dominates and winds are mild.

Yang et al. [191] implemented a modified air curtain that reduced thermal loss from 100 W to 10 W as tilt increased from 0° to 90° at 723 K. Alipourtarzanagh et al. [180] showed that at 30° and in calm ambient, increasing curtain velocity cut convective loss by up to 60%, with benefits declining in wind; in related tests, Alipourtarzanagh et al. [192] found suction to outperform blowing by 47% under zero wind. Cheilytko and Schwarzbözl [193] introduced a receiver with a returned air vortex and reported a 4% increase in air return coefficient and further convection reductions as returned air axial velocity increased. Fang et al. [194] optimized nozzle inclination, thickness, jet temperature, and velocity to achieve up to 28.6% convective loss reduction, and Zhang et al. [195] validated comparable setups with up to 45% reduction.

Collectively, well-designed secondary flow systems, air curtains, suction, and returned air vortex concepts can reduce convective losses by 28.6–60% under favorable conditions, with documented cases ranging from 100 W down to 10 W. Performance depends on tilt, wind, and nozzle parameters; suction and higher returned air velocities are particularly effective when ambient winds are low.

7.3.3. Other innovative solutions

Beyond fins and air curtains, several concepts act through optical add-ons, porous structures, advanced materials, and modified geometry or kinematics.

Wang et al. [196] used spillage skirts and secondary reflectors on a cylindrical receiver, achieving a 1.3% efficiency increase and a 12.7% total loss reduction relative to a simple cylinder. Meng et al. [197] designed a hemispherical–cylindrical hybrid with Al_2O_3 and SiC porous absorbers and showed that increasing HTF flow rate markedly reduces shell radiation, with SiC incurring higher losses than Al_2O_3. Wan et al. [198] placed porous shroud walls around the aperture and observed nearly 53% lower convective loss across wind directions and cavity shapes.

Li et al. [182] applied a 0.01 m SiO_2 aerogel layer and achieved a 22.8% total loss reduction at 90° inclination in fully passive operation. Nandanwar and Walke [181] filled a conical receiver with PCM, increasing thermal efficiency by 42% and lowering total loss by up to 56%. Na et al. [183] evaluated a positive conical cavity, radiation entering the smaller face, at 450–750 K and −90° to 90° inclinations and showed that at 750 K and downward facing, thermal loss was 9.2, 14.3, and 14.11 times lower than in cylindrical, hemispherical, and typical conical receivers. Fan et al. [199] integrated a parabolic dish with a conical cavity and reported 2.7–27.5% performance gains and a 6% loss reduction versus conventional absorbers. Kopalakrishnaswami and Natarajan [200] achieved 84.7% efficiency at 400 °C with a modified conical receiver, outperforming a modified cavity, 83.5%, a conventional cone, 71.5%, and a cylinder, 67.3%, and showing nearly sixfold lower thermal loss at 45°.

In sum, optical add-ons, porous structures, aerogels, PCMs, and modified geometry or kinematics deliver 1.3–27.5% efficiency improvements and up to 56% total loss reduction, with special geometries achieving order-of-magnitude lower losses under specific conditions. Selection should align with the dominant loss mechanism, whether radiation or convection, the temperature range, inclination, wind exposure, and acceptable design complexity.

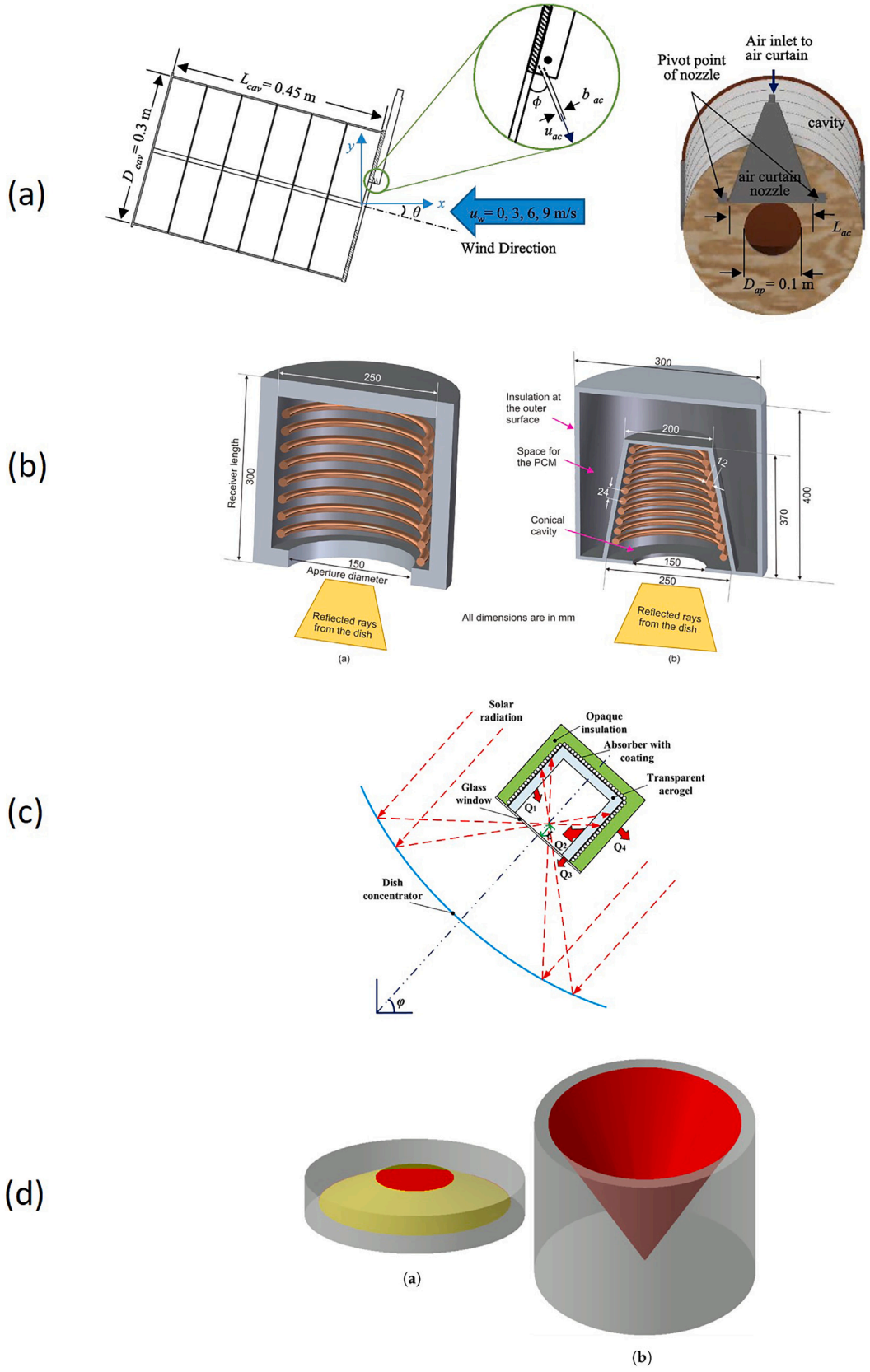


Fig. 13. Mitigation strategies: (a) air curtains [180], (b) PCM [181], (c) aerogel [182], (d) positive conical cavity receiver [183]. (Obtained with permission from Alipourtarzanagh et al. [180] and Li et al. [182]).

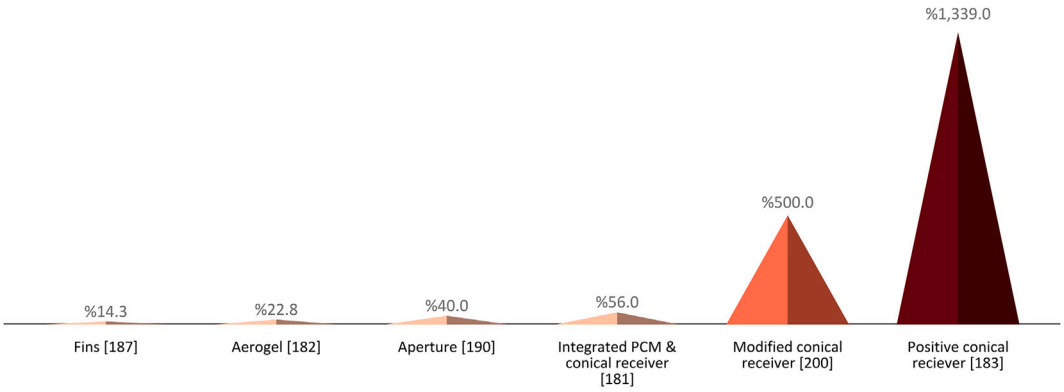


Fig. 14. Total thermal loss reduction (%) achieved by implementing different modification strategies in cavity receivers; Fins [187], Aerogel [182] Aperture [190], PCM [181], modified conical receiver [200], conical positive receiver [183].

7.3.4. Which thermal loss mitigation strategy is better?

Fig. 14 compares maximum total loss reductions across strategies. Adding fins lowers total loss by up to 14.32% in hemispherical cavities [187], whereas aperture glazing achieves as much as 37.97% reduction [190]. Advanced materials alone reduce losses by up to 22.8%, for example a 0.01 m SiO_2 aerogel layer [182], and when integrated with geometrical modifications, such as PCM-filled conical receivers, the total reduction can reach 56% [181]. Innovative cavity receiver designs deliver step-change benefits, roughly 6–14 times lower total loss than conventional cavities under comparable conditions [183,200], so exploring new receiver architectures is a promising pathway to minimize losses and improve efficiency simultaneously.

8. Opportunities, major issues, challenges, and recommended future work

CSP plants, particularly point-focus systems, are central to renewable energy expansion. Despite higher capital costs than photovoltaics, they generally achieve higher electricity-generation efficiency [201,202] and, with integrated thermal storage, provide dispatchable power without sunlight, whereas PV requires costly electrochemical storage for comparable continuity [203–208]. High operating temperatures and large thermal throughputs also enable industrial applications such as hydrogen and ammonia synthesis and aluminum production [209–212], yet thermal losses remain a primary constraint on receiver and plant performance.

Based on the synthesis in the preceding sections, the following gaps emerge as actionable findings that limit predictive design and cross-study comparability:

- **F1 (Comparability):** Key boundary conditions are inconsistently reported (wind speed/direction, tilt/yaw conventions, flux non-uniformity, emissivity/view factor assumptions, and uncertainty), preventing reliable cross-study normalization.
- **F2 (Regime identification):** Mixed convection is often discussed qualitatively; the governing regime is rarely reported in a transferable way, contributing to conflicting trends across studies and limiting the portability of correlations.
- **F3 (Coupled losses):** Relatively few studies quantify convective and radiative losses over the same operating envelope, limiting identification of when geometry/flow control versus surface engineering is the dominant lever.
- **F4 (Validation gap):** Tower-mounted receivers remain dominated by numerical evidence, with limited validated datasets at relevant scales and wind exposures.

For external receivers, environmental effects are widely explored numerically, but experimental validation remains limited. Full-scale tests are expensive, whereas scaled wind tunnel experiments are feasible and underutilized for validating thermal loss models. To reduce the validation gap, coordinated campaigns should adopt a minimum common test matrix for both external and cavity archetypes: at least three surface temperature levels spanning the convection- to radiation-dominated transition, at least three orientations with a clearly stated sign convention, and multiple wind conditions (including head-on and side-on) with documented turbulence intensity. Reporting should include partitioned losses (Q_{conv}, Q_{rad}, Q_{cond}), surface emissivity and view factor treatment (or an effective-emissivity definition for cavities), the applied heat flux boundary condition (uniform or mapped non-uniform), and uncertainty bounds. Standardized reporting enables correlation transfer, model validation, and meta-analysis across laboratories and geometries.

In parallel, progress in advanced materials, including nanofluids as HTFs, PCMs for thermal recovery, and high temperature coatings and bulk materials, is essential for next generation operating conditions. Geometrical modifications have been studied, but optimization of internal HTF passages in cylindrical and flat tower receivers remains comparatively underdeveloped, particularly when constraints from peak flux, allowable tube temperature, and thermomechanical limits are imposed alongside heat loss minimization.

Cavity receivers allow more affordable testing, yielding a larger experimental base for parabolic dish systems, while tower-mounted cavities remain dominated by numerical studies and would benefit from carefully designed experiments. As with external receivers, improved working fluids and high temperature coatings are crucial for durable, low loss operation. Because cavity losses are aperture-controlled, strategies that jointly manage reradiation and aperture-driven air exchange (e.g., aperture treatments, shielding, and flow-control concepts) should be evaluated under standardized windy and tilted conditions to establish transferable performance bounds.

The trade-off between convective and radiative losses remains unresolved, with relatively few studies that decouple or jointly quantify both mechanisms across temperature, inclination, wind, and aperture conditions. Bridging this gap is critical for prioritizing mitigation. Mature measures such as aperture glazing coexist with less systematically explored options, including aerogel-based insulation, architected porous structures, and novel geometries, which can reduce losses in both external and cavity receivers. Targeted campaigns that map operating regimes to the dominant loss pathway would improve transferability and accelerate design convergence.

AI and data-driven methods are most valuable where repeated high-fidelity simulation (CFD coupled with radiation and conduction) is too costly for design-space exploration. A practical pathway is to build surrogate models trained on curated, validated datasets, with inputs encoding geometry (e.g., aperture ratio, aspect ratio, shielding), operating conditions (temperature, mass flow, wind speed/direction, orientation),

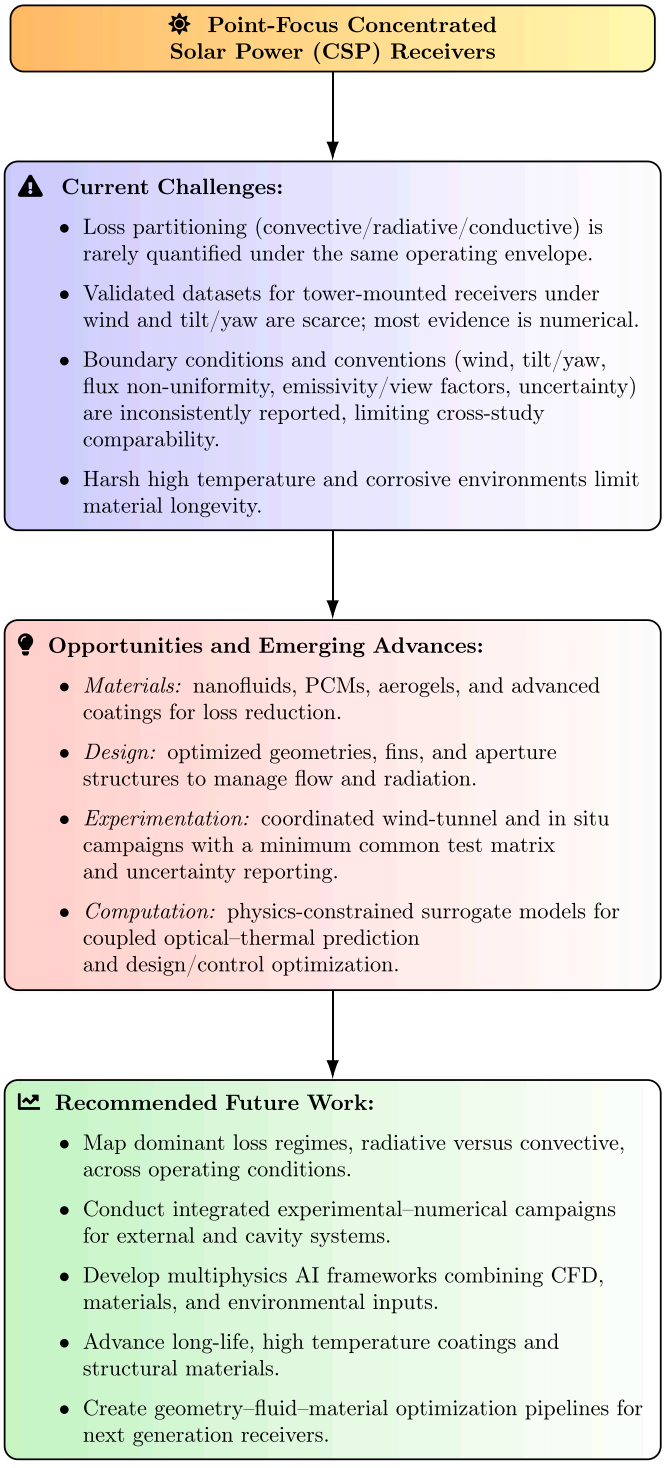


Fig. 15. Conceptual framework summarizing opportunities, challenges, and research directions for point-focus CSP receivers.

and surface properties (emissivity/absorptivity), and outputs predicting partitioned losses and receiver efficiency. Physics-constrained regression or physics-informed machine learning can preserve known scaling (e.g., radiative T^4 dependence) while learning correction factors across mixed-convection regimes. These surrogates enable rapid geometry, fluid, and material optimization and can be embedded in operational strategies (e.g., mass flow scheduling using DNI forecasts) to reduce peak temperatures and losses under realistic operation.

Fig. 15 summarizes these findings and translates them into prioritized research actions spanning experiments, computation, design, and materials.

9. Conclusion

This review surveys research that analyzes thermal losses as a determinant of performance in point-focus CSP systems, cavity and external receivers, and research that targets losses and proposes mitigation across the main heat dissipation modes to increase efficiency.

Although only a limited set of parameters directly governs thermal efficiency, many factors that influence or mitigate thermal losses indirectly shape performance. Prioritizing thermal loss-related parameters is therefore a promising route to improvement. Thermal losses in cavity receivers have been studied extensively, whereas external receivers have received less attention; given the impact of losses on efficiency, there is a clear need to deepen understanding and develop integrated mitigation strategies. Progress will require coordinated in situ experimentation, exploration of new geometries and materials, and designs that address multiple loss mechanisms concurrently.

This review has limitations. Data availability and quality, particularly for environmental conditions such as temperature, humidity, and wind speed, constrained sensitivity assessment and limited comparability across studies. These gaps motivate a research agenda that couples rigorous experimentation with high-fidelity modeling, advances materials and geometric design for high temperature operation, and integrates mitigation across convective, radiative, and conductive pathways, aiming for systematic optimization of point-focus CSP performance.

CRediT authorship contribution statement

Pedram Alamdari: Writing – review & editing, Writing – original draft, Visualization, Validation, Investigation, Formal analysis, Data curation, Conceptualization. **Mehdi Khatamifar:** Writing – review & editing, Supervision. **Wenxian Lin:** Writing – review & editing, Supervision.

Declaration of generative AI and AI-assisted technologies in the manuscript preparation process

During the preparation of this work, the authors used ChatGPT in order to check grammar and writing style. After using this tool/service, the authors reviewed and edited the content as needed and took full responsibility for the content of the published article.

Declaration of competing interest

The authors declare that they have no known competing financial interests or personal relationships that could have appeared to influence the work reported in this paper.

Acknowledgment

The authors would like to thank Associate Professor Juan Felipe Torres of the Australian National University for his valuable advice, which significantly improved this review.

Appendix A. Inputs used to generate Fig. 12

See (Table A.1).

Table A.1
Parameters used in selected Nusselt correlations and their reported ranges.

Ref	Used parameter in the Nusselt correlation	Range
Yazdanipour et al. [109] Upward-facing cylindrical receiver	θ	−90°
	T_w/T_∞	1.6
	Ra	$1.11\times10^8 - 1.86\times10^8$
Yazdanipour et al. [109] Side-facing cylindrical receiver	θ	0°
	T_w/T_∞	1.8
	Ra	$8.31\times10^7 - 1.44\times10^8$
Sharma and Saha [100] Upward-facing conical receiver	γ	30°
	T_w/T_∞	1.2
	Pr	1
	Ra	$1.52\times10^8 - 2.0\times10^8$
Sharma and Saha [100] Upward-facing cylindrical receiver	T_w/T_∞	1.2
	Pr	1
	D/H	1
	Ra	$5.00\times10^7 - 3.9\times10^8$
Vikram and Reddy [149] Side-facing hemispherical receiver	T_w/T_∞	1.79
	Pr	0.71
	θ	0°
	ε	0
	A_w/A_1	1.845
	N_{rc}	130.64
	λ	0.00694
	Ra	$6.1\times10^7 - 7.31\times10^8$
Jilte et al. [96] Side-facing cylindrical receiver	θ	0°
	T_w/T_∞	2.3
	Ra	$1.04\times10^7 - 1.56\times10^8$
Tan et al. [154] Side-facing hemispherical receiver	θ	0°
	T_w/T_∞	1.5
	D/D_a	0.43
	Ra	$1.35\times10^8 - 1.99\times10^8$
	Pr	0.71

Data availability

No data was used for the research described in the article.

References

[1] M. Osman, I. Qureshi, Review of photovoltaic and concentrated solar technologies including their performance, reliability, efficiency and storage, Results Eng. 25 (2025) 104424, https://doi.org/10.1016/j.rineng.2025.104424, https://www.sciencedirect.com/science/article/pii/S2590123025005031.

[2] K. Ukoba, K.O. Yoro, O. Eterigho-Ikelegbe, C. Ibegbulam, T.-C. Jen, Adaptation of solar energy in the global south: Prospects, challenges and opportunities, Heliyon 10 (7) (2024) e28009, https://doi.org/10.1016/j.heliyon.2024.e28009, https://www.sciencedirect.com/science/article/pii/S2405844024040404.

[3] World Bank Group, Global solar atlas-map and data downloads, 2025 https://globalsolaratlas.info/download/world (Accessed: 24 October 2025).

[4] International Energy Agency, International energy agency (IEA), https://www.iea.org/countries/ (Accessed: 24 October 2025).

[5] International Energy Agency, International energy agency (IEA), https://www.iea.org/reports/gas-market-report-q1-2026 (Accessed: 24 October 2025).

[6] M.J. Blanco, S. Miller, 1 - Introduction to concentrating solar thermal (CST) technologies, In M.J. Blanco, L.R. Santigosa (Eds.), Advances in Concentrating Solar Thermal Research and Technology, Woodhead Publishing, 2017, pp. 3–25, https://doi.org/10.1016/B978-0-08-100516-3.00001-0, Woodhead Publishing Series in Energy

[7] M. Caccia, M. Tabandeh-Khorshid, G. Itskos, A. Strayer, A. Caldwell, S. Pidaparti, S. Singnisai, A. Rohskopf, A. Schroeder, D. Jarrahbashi, T. Kang, S. Sahoo, K. Naveen, A. Marquez-Rossy, M. Anderson, E. Lara-Curzio, D. Ranjan, A. Henry, K. Sandhage, Ceramic–metal composites for heat exchangers in concentrated solar power plants, Nature 562 (2018) 406–409, https://doi.org/10.1038/s41586-018-0593-1

[8] C. Wu, Z. Hou, Z. Wang, Doping nanoparticles to enhance the thermal properties of eutectic salts in high temperature latent heat storage systems: A comprehensive review, Int. J. Heat Mass Transf. 240 (2025) 126677, https://doi.org/10.1016/j.ijheatmasstransfer.2025.126677, https://www.sciencedirect.com/science/article/pii/S0017931025000183.

[9] A.A. Hachicha, B.A.A. Yousef, Z. Said, I. Rodríguez, A review study on the modeling of high-temperature solar thermal collector systems, Renew. Sustain. Energy Rev. 112 (2019) 280–298, https://doi.org/10.1016/j.rser.2019.05.056, https://www.sciencedirect.com/science/article/pii/S136403211930379X.

[10] W. Fuqiang, C. Ziming, T. Jianyu, Y. Yuan, S. Yong, L. Linhua, Progress in concentrated solar power technology with parabolic trough collector system: A comprehensive review, Renew. Sustain. Energy Rev. 79 (2017) 1314–1328, https://doi.org/10.1016/j.rser.2017.05.174, https://www.sciencedirect.com/science/article/pii/S1364032117308122.

[11] P. del Río, C. Peñasco, P. Mir-Artigues, An overview of drivers and barriers to concentrated solar power in the European Union, Renew. Sustain. Energy Rev. 81 (2018) 1019–1029, https://doi.org/10.1016/j.rser.2017.06.038, https://www.sciencedirect.com/science/article/pii/S1364032117309784.

[12] National Renewable Energy Laboratory, Concentrating solar power projects, 2025 https://solarpaces.nrel.gov/projects (Accessed: 12 March 2025).

[13] J. Kim, J.-S. Kim, W. Stein, Simplified heat loss model for central tower solar receiver, Sol. Energy 116 (2015) 314–322, https://doi.org/10.1016/j.solener.2015.02.022, https://www.sciencedirect.com/science/article/pii/S0038092X15000924.

[14] S. Yang, L. Li, B. Wang, Y. Zheng, P. Lund, J. Wang, Y. Ding, Modelling of radiative and convective heat transfer in an open cavity volumetric receiver for a 50-MWth beam-down integrated receiver-storage concentrating solar thermal system, Renew. Energy 242 (2025) 122457, https://doi.org/10.1016/j.renene.2025.122457, https://www.sciencedirect.com/science/article/pii/S0960148125001193.

[15] A. Albarbar, A. Arar, Performance assessment and improvement of central receivers used for solar thermal plants, Energies 12 (2019) 3079, https://doi.org/10.3390/en12163079, https://www.mdpi.com/1996-1073/12/16/3079.

[16] A.M. Clausing, An analysis of convective losses from cavity solar central receivers, Sol. Energy 27 (1981) 295–300, https://doi.org/10.1016/0038-092X(81)90062-1, https://www.sciencedirect.com/science/article/pii/0038092X81900621.

[17] A.M. Clausing, Convective losses from cavity solar receivers—comparisons between analytical predictions and experimental results, J. Sol. Energy Eng. 105 (1983) 29–33, https://doi.org/10.1115/1.3266342, https://asmedigitalcollection.asme.org/solarenergyengineering/article-pdf/105/1/29/5535414/29_1.pdf.

[18] A.M. Clausing, J.M. Waldvogel, L.D. Lister, Natural convection from isothermal cubical cavities with a variety of side-facing apertures, J. Heat Transf. 109 (1987) 407–412, https://doi.org/10.1115/1.3248095, https://asmedigitalcollection.asme.org/heattransfer/article-pdf/109/2/407/5636870/407_1.pdf.

[19] J.A. Harris, T.G. Lenz, Thermal performance of solar concentrator/cavity receiver systems, Sol. Energy 34 (1985) 135–142, https://doi.org/10.1016/0038-092X(85)90170-7, https://www.sciencedirect.com/science/article/pii/0038092X85901707.

[20] S.W. Churchill, A comprehensive correlating equation for laminar, assisting, forced and free convection, Aiche J. 23 (1977) 10–16, https://doi.org/10.1002/aic.690230103, https://aiche.onlinelibrary.wiley.com/doi/pdf/10.1002/aic.690230103.

[21] D.L. Siebers, R.G. Schwind, R.J. Moffat, Experimental mixed-convection heat transfer from a large, vertical surface in a horizontal flow, Tech. rep., Sandia National Labs, Livermore, CA (USA); Nielsen Engineering and Research, Inc, Mountain View, CA (USA); Stanford Univ, CA (USA) (Jul 1983, https://doi.org/10.2172/5873492. https://www.osti.gov/biblio/5873492.

[22] D.L. Siebers, J.S. Kraabel, Estimating convective energy losses from solar central receivers, Tech. Report SAND84-8717, Sandia National Lab, Livermore, CA, United States, 1984, https://doi.org/10.2172/6906848. https://www.osti.gov/biblio/6906848.

[23] A.O.M. Maka, T.S. O'Donovan, A review of thermal load and performance characterisation of a high concentrating photovoltaic (hcpv) solar receiver assembly, Sol. Energy 206 (2020) 35–51, https://doi.org/10.1016/j.solener.2020.05.022, https://www.sciencedirect.com/science/article/pii/S0038092X20305119.

[24] M.M. Khademi, A. Kasaeian, Hydrogen production using solar heliostat fields: A review, Energy 314 (2025) 134259, https://doi.org/10.1016/j.energy.2024.134259, https://www.sciencedirect.com/science/article/pii/S0360544224040374.

[25] F. Yilmaz, M. Ozturk, R. Selbas, Proposal of an advanced hybrid multigeneration plant using solar energy for sustainable hydrogen generation: A thermodynamic and environmental analysis, Renew. Energy 243 (2025) 122621, https://doi.org/10.1016/j.renene.2025.122621, https://www.sciencedirect.com/science/article/pii/S0960148125002836.

[26] X. Han, L. Wang, H. Ling, Z. Ge, X. Lin, X. Dai, H. Chen, Critical review of thermochemical energy storage systems based on cobalt, manganese, and copper oxides, Renew. Sustain. Energy Rev. 158 (2022) 112076, https://doi.org/10.1016/j.rser.2022.112076, https://www.sciencedirect.com/science/article/pii/S1364032122000065.

[27] X. Xu, K. Vignarooban, B. Xu, K. Hsu, A.M. Kannan, Prospects and problems of concentrating solar power technologies for power generation in the desert regions, Renew. Sustain. Energy Rev. 53 (2016) 1106–1131, https://doi.org/10.1016/j.rser.2015.09.015, https://www.sciencedirect.com/science/article/pii/S1364032115009855.

[28] L.L. Vant-Hull, 8 - central tower concentrating solar power (CSP) systems, In K. Lovegrove, W. Stein (Eds.), Concentrating Solar Power Technology, Woodhead Publishing, 2012, pp. 240–283, https://doi.org/10.1533/9780857096173.2.240, Woodhead Publishing Series in Energy
[29] C.K. Ho, J.M. Christian, J.D. Ortega, J. Yellowhair, M.J. Mosquera, C.E. Andraka, Reduction of radiative heat losses for solar thermal receivers, in: A.P. Plesniak, C. Pfefferkorn (Eds.), High and Low Concentrator Systems for Solar Energy Applications IX, vol. 9175, International Society for Optics and Photonics, SPIE, 2014, p. 917506. https://doi.org/10.1117/12.2063152
[30] M. Cagnoli, A. de la Calle, J. Pye, L. Savoldi, R. Zanino, A CFD-supported dynamic system-level model of a sodium-cooled billboard-type receiver for central tower CSP applications, Sol. Energy 177 (2019) 576–594, https://doi.org/10.1016/j.solener.2018.11.031, https://www.sciencedirect.com/science/article/pii/S0038092X18311320.
[31] Y. Wang, M. Zheng, J.F. Torres, A. Shirazi, J. Coventry, J. Pye, Integrated optical–thermal modelling and techno-economic evaluation of a 'bladed'solar-thermal receiver, Sol. Energy 266 (2023) 112027.
[32] J.F. Torres, K. Tsuda, Y. Murakami, Y. Guo, S. Hosseini, C.-A. Asselineau, M. Taheri, K. Drewes, A. Tricoli, W. Lipiński, J. Coventry, Highly efficient and durable solar thermal energy harvesting via scalable hierarchical coatings inspired by stony corals, Energy Environ. Sci. 15 (5) (2022) 1893–1906.
[33] Y. Guo, K. Tsuda, M. Mohsenzadeh, S. Hosseini, Y. Murakami, J. Coventry, J.F. Torres, Titania-based coral-structured solar absorber coating with improved scalability and durability at high temperature, Adv. Sci. 11 (42) (2024) 2407409.
[34] Y. Guo, K. Tsuda, S. Hosseini, Y. Murakami, A. Tricoli, J. Coventry, W. Lipiński, J.F. Torres, Scalable nano-architecture for stable near-blackbody solar absorption at high temperatures, Nat. Commun. 15 (1) (2024) 384.
[35] C.K. Ho, B.D. Iverson, Review of high-temperature central receiver designs for concentrating solar power, Renew. Sustain. Energy Rev. 29 (2014) 835–846, https://doi.org/10.1016/j.rser.2013.08.099, https://www.sciencedirect.com/science/article/pii/S1364032113006394.
[36] A. Kasaeian, A. Kouravand, M.A. Vaziri Rad, S. Maniee, F. Pourfayaz, Cavity receivers in solar dish collectors: A geometric overview, Renew. Energy 169 (2021) 53–79, https://doi.org/10.1016/j.renene.2020.12.106, https://www.sciencedirect.com/science/article/pii/S0960148120320462.
[37] M.I. Khan, F. Asfand, S.G. Al-Ghamdi, Progress in research and technological advancements of commercial concentrated solar thermal power plants, Sol. Energy 249 (2023) 183–226, https://doi.org/10.1016/j.solener.2022.10.041, https://www.sciencedirect.com/science/article/pii/S0038092X22007800.
[38] M.I. Alam, M.M. Nuhash, A. Zihad, T.H. Nakib, M.M. Ehsan, Conventional and emerging CSP technologies and design modifications: Research status and recent advancements, Int. J. Thermofluids 20 (2023) 100406, https://doi.org/10.1016/j.ijft.2023.100406, https://www.sciencedirect.com/science/article/pii/S2666202723001234.
[39] I. Arias, J. Cardemil, E. Zarza, L. Valenzuela, R. Escobar, Latest developments, assessments and research trends for next generation of concentrated solar power plants using liquid heat transfer fluids, Renew. Sustain. Energy Rev. 168 (2022) 112844, https://doi.org/10.1016/j.rser.2022.112844, https://www.sciencedirect.com/science/article/pii/S1364032122007262.
[40] X. Li, F. Bai, A review on the thermal modeling method for molten salt receivers of concentrating solar power tower plants, Energies 18 (2) (2025) 292, https://doi.org/10.3390/en18020292, https://www.mdpi.com/1996-1073/18/2/292.
[41] A.A. Rizvi, S.N. Danish, A. El-Leathy, H. Al-Ansary, D. Yang, A review and classification of layouts and optimization techniques used in design of heliostat fields in solar central receiver systems, Sol. Energy 218 (2021) 296–311, https://doi.org/10.1016/j.solener.2021.02.011, https://www.sciencedirect.com/science/article/pii/S0038092X21001122.
[42] A.N. Yerudkar, D. Kumar, V.H. Dalvi, S.V. Panse, V.R. Gaval, J.B. Joshi, Economically feasible solutions in concentrating solar power technology specifically for heliostats – a review, Renew. Sustain. Energy Rev. 189 (2024) 113825, https://doi.org/10.1016/j.rser.2023.113825, https://www.sciencedirect.com/science/article/pii/S1364032123006822.
[43] J.C. Sattler, M. Röger, P. Schwarzbözl, R. Buck, A. Macke, C. Raeder, J. Göttsche, Review of heliostat calibration and tracking control methods, Sol. Energy 207 (2020) 110–132, https://doi.org/10.1016/j.solener.2020.06.030, https://www.sciencedirect.com/science/article/pii/S0038092X20306447.
[44] M. Maiga, K.E. N'Tsoukpoe, A. Gomna, Y.K. Fiagbe, Sources of solar tracking errors and correction strategies for heliostats, Renew. Sustain. Energy Rev. 203 (2024) 114770, https://doi.org/10.1016/j.rser.2024.114770, https://www.sciencedirect.com/science/article/pii/S1364032124004969.
[45] D. Hering, M. Binder, P. Schwarzbözl, R. Schwaiger, R. Pitz-Paal, Monitoring of service life consumption for tubular solar receivers: Review of contemporary thermo-mechanical and damage modeling approaches, Sol. Energy 226 (2021) 427–445, https://doi.org/10.1016/j.solener.2021.08.022, https://www.sciencedirect.com/science/article/pii/S0038092X21006770.
[46] S. Dosta, L. Betancor, C. Barreneche, Overview of surface engineering technology to improve the energy efficiency in concentrated solar power (CSP) plants, Sol. Energy Mater. Sol. Cells 277 (2024) 113090, https://doi.org/10.1016/j.solmat.2024.113090, https://www.sciencedirect.com/science/article/pii/S0927024824004021.
[47] M.E. Zayed, J. Zhao, A.H. Elsheikh, W. Li, S. Sadek, M.M. Aboelmaaref, A comprehensive review on dish/stirling concentrated solar power systems: Design, optical and geometrical analyses, thermal performance assessment, and applications, J. Clean. Prod. 283 (2021) 124664, https://doi.org/10.1016/j.jclepro.2020.124664, https://www.sciencedirect.com/science/article/pii/S0959652620347089.
[48] M.Z. Malik, P.H. Shaikh, S. Zhang, A.A. Lashari, Z.H. Leghari, M.H. Baloch, Z.A. Memon, C. Caiming, A review on design parameters and specifications of parabolic solar dish stirling systems and their applications, Energy Rep. 8 (2022) 4128–4154, https://doi.org/10.1016/j.egyr.2022.03.031, https://www.sciencedirect.com/science/article/pii/S2352484722005868.
[49] T. Conroy, M.N. Collins, R. Grimes, A review of steady-state thermal and mechanical modelling on tubular solar receivers, Renew. Sustain. Energy Rev. 119 (2020) 109591, https://doi.org/10.1016/j.rser.2019.109591, https://www.sciencedirect.com/science/article/pii/S1364032119307993.
[50] R.P. Merchán, M.J. Santos, A. Medina, A. Calvo Hernández, High temperature central tower plants for concentrated solar power: 2021 overview, Renew. Sustain. Energy Rev. 155 (2022) 111828, https://doi.org/10.1016/j.rser.2021.111828, https://www.sciencedirect.com/science/article/pii/S1364032121010923.
[51] D. Jafrancesco, J.P. Cardoso, A. Mutuberria, E. Leonardi, I. Les, P. Sansoni, F. Francini, D. Fontani, Optical simulation of a central receiver system: Comparison of different software tools, Renew. Sustain. Energy Rev. 94 (2018) 792–803, https://doi.org/10.1016/j.rser.2018.06.028, https://www.sciencedirect.com/science/article/pii/S1364032118304647.
[52] W. Lipiński, E. Abbasi-Shavazi, J. Chen, J. Coventry, M. Hangi, S. Iyer, A. Kumar, L. Li, S. Li, J. Pye, J.F. Torres, B. Wang, Y. Wang, V.M. Wheeler, Progress in heat transfer research for high-temperature solar thermal applications, Appl. Therm. Eng. 184 (2021) 116137, https://doi.org/10.1016/j.applthermaleng.2020.116137, https://www.sciencedirect.com/science/article/pii/S1359431120336176.
[53] K. Milidonis, M.J. Blanco, V. Grigoriev, C.F. Panagiotou, A.M. Bonanos, M. Constantinou, J. Pye, C.-A. Asselineau, Review of application of AI techniques to solar tower systems, Sol. Energy 224 (2021) 500–515, https://doi.org/10.1016/j.solener.2021.06.009, https://www.sciencedirect.com/science/article/pii/S0038092X21004825.
[54] Y.-L. He, K. Wang, Y. Qiu, B.-C. Du, Q. Liang, S. Du, Review of the solar flux distribution in concentrated solar power: Non-uniform features, challenges, and solutions, Appl. Therm. Eng. 149 (2019) 448–474, https://doi.org/10.1016/j.applthermaleng.2018.12.006, https://www.sciencedirect.com/science/article/pii/S1359431118360769.
[55] K.H. Kumar, A.M. Daabo, M.K. Karmakar, et al., Solar parabolic dish collector for concentrated solar thermal systems: a review and recommendations, Environ. Sci. Pollut. Res. 29 (47) (2022) 32335–32367, https://doi.org/10.1007/s11356-022-18586-4
[56] Y.N. Nandanwar, P.V. Walke, A comprehensive review on integration of receiver geometries, nanofluids, and efficient thermal energy storage for solar parabolic dish collectors, J. Braz. Soc. Mech. Sci. Eng. 46 (8) (2024) 480, published online 2024-06-28. https://doi.org/10.1007/s40430-024-05034-2
[57] A.L. Avila-Marin, J. Fernandez-Reche, A. Martinez-Tarifa, Modelling strategies for porous structures as solar receivers in central receiver systems: A review, Renew. Sustain. Energy Rev. 111 (2019) 15–33, https://doi.org/10.1016/j.rser.2019.03.059, https://www.sciencedirect.com/science/article/pii/S1364032119301996.
[58] J. Coventry, C. Andraka, J. Pye, M. Blanco, J. Fisher, A review of sodium receiver technologies for central receiver solar power plants, Sol. Energy 122 (2015) 749–762, https://doi.org/10.1016/j.solener.2015.09.023, https://www.sciencedirect.com/science/article/pii/S0038092X15005083.
[59] H.A. Aljaerani, M. Samykano, R. Saidur, A.K. Pandey, K. Kadirgama, Nanoparticles as molten salts thermophysical properties enhancer for concentrated solar power: A critical review, J. Energy Storage 44 (2021) 103280, https://doi.org/10.1016/j.est.2021.103280, https://www.sciencedirect.com/science/article/pii/S2352152X21009737.
[60] B. Liu, L. Wenhao, L. Zhenmin, S. Sarvar, L. Fereidooni, A. Kasaeian, Performance improving of concentrated solar power systems with nanofluids: A review based on molecular dynamics, J. Mol. Liq. 414 (2024) 126052, https://doi.org/10.1016/j.molliq.2024.126052, https://www.sciencedirect.com/science/article/pii/S0167732224021111.
[61] M. Lambrecht, M.T. de Miguel, M.I. Lasanta, F.J. Pérez, Past research and future strategies for molten chlorides application in concentrated solar power technology, Sol. Energy Mater. Sol. Cells 237 (2022) 111557, https://doi.org/10.1016/j.solmat.2021.111557, https://www.sciencedirect.com/science/article/pii/S0927024821005912.
[62] N. Hanrieder, S. Wilbert, D. Mancera-Guevara, R. Buck, S. Giuliano, R. Pitz-Paal, Atmospheric extinction in solar tower plants – a review, Sol. Energy 152 (2017) 193–207, progress in Solar Energy Special Issue: Concentrating Solar Power (CSP). https://doi.org/10.1016/j.solener.2017.01.013, https://www.sciencedirect.com/science/article/pii/S0038092X17300221.
[63] J. Samanes, J. García-Barberena, F. Zaversky, Modeling solar cavity receivers: A review and comparison of natural convection heat loss correlations, Energy Procedia 69 (2015) 543–552, International Conference on Concentrating Solar Power and Chemical Energy Systems, SolarPACES 2014. https://doi.org/10.1016/j.egypro.2015.03.063, https://www.sciencedirect.com/science/article/pii/S1876610215003690.
[64] A.A. Abed, M.R. El-Marghany, W.M. El-Awady, A.M. Hamed, Recent advances in parabolic dish solar concentrators: Receiver design, heat loss reduction, and nanofluid optimization for enhanced efficiency and applications, Sol. Energy Mater. Sol. Cells 273 (2024) 112930, https://doi.org/10.1016/j.solmat.2024.112930, https://www.sciencedirect.com/science/article/pii/S0927024824002423.
[65] K. Wasankar, N. Gulhane, Review of various solar cavity receivers of parabolic dish concentrators with design aspects and heat loss analysis, J. Therm. Eng. 10 (3) (2024) 756–772, https://doi.org/10.14744/thermal.0000810

[66] P. Alamdari, M. Khatamifar, W. Lin, Heat loss analysis review: Parabolic trough and linear fresnel collectors, Renew. Sustain. Energy Rev. 199 (2024) 114497, https://doi.org/10.1016/j.rser.2024.114497, https://www.sciencedirect.com/science/article/pii/S136403212400220X.
[67] J.M. Christian, C.K. Ho, CFD simulation and heat loss analysis of the Solar Two Power Tower receiver, in: ASME 2012 6th International Conference on Energy Sustainability, Parts A and B of Energy Sustainability, 2012, pp. 227–235, https://doi.org/10.1115/ES2012-91030, https://asmedigitalcollection.asme.org/ES/proceedings-pdf/ES2012/44816/227/4447530/227_1.pdf.
[68] B.S. Emerick, F.G. Battisti, A.K. da Silva, Geometric optimization of a solar tower receiver operating with supercritical CO_2 as working fluid, Appl. Therm. Eng. 228 (2023) 120318, https://doi.org/10.1016/j.applthermaleng.2023.120318, https://www.sciencedirect.com/science/article/pii/S1359431123003472.
[69] Q. Zhang, D. Cao, Z. Ge, X. Du, Response characteristics of external receiver for concentrated solar power to disturbance during operation, Appl. Energy 278 (2020) 115709, https://doi.org/10.1016/j.apenergy.2020.115709, https://www.sciencedirect.com/science/article/pii/S0306261920312034.
[70] M.A. Qaisrani, J. Wei, J. Fang, Y. Jin, Z. Wan, M. Khalid, Heat losses and thermal stresses of an external cylindrical water/steam solar tower receiver, Appl. Therm. Eng. 163 (2019) 114241, https://doi.org/10.1016/j.applthermaleng.2019.114241, https://www.sciencedirect.com/science/article/pii/S135943111931347X.
[71] J.F. Torres, F. Ghanadi, I. Nock, M. Arjomandi, J. Pye, Mixed convection around a tilted cuboid with an isothermal sidewall at moderate reynolds numbers, Int. J. Heat Mass Transf. 119 (2018) 418–432, https://doi.org/10.1016/j.ijheatmasstransfer.2017.11.109, https://www.sciencedirect.com/science/article/pii/S0017931017340310.
[72] M.A. Qaisrani, J. Fang, Y. Jin, Z. Wan, N. Tu, M. Khalid, M.U. Rahman, J. Wei, Thermal losses evaluation of an external rectangular receiver in a windy environment, Sol. Energy 184 (2019) 281–291, https://doi.org/10.1016/j.solener.2019.03.103, https://www.sciencedirect.com/science/article/pii/S0038092X19303317.
[73] V. Thirunavukkarasu, M. Cheralathan, An experimental study on energy and exergy performance of a spiral tube receiver for solar parabolic dish concentrator, Energy 192 (2020) 116635, https://doi.org/10.1016/j.energy.2019.116635, https://www.sciencedirect.com/science/article/pii/S0360544219323308.
[74] S.K. Vishnu, R. Senthil, Experimental performance evaluation of a solar parabolic dish collector using spiral flow path receiver, Appl. Therm. Eng. 231 (2023) 120979, https://doi.org/10.1016/j.applthermaleng.2023.120979, https://www.sciencedirect.com/science/article/pii/S1359431123010086.
[75] E. Vengadesan, P. Gurusamy, R. Senthil, Thermal performance analysis of flat surface solar receiver with square tubular fins for a parabolic dish collector, Renew. Energy 216 (2023) 119048, https://doi.org/10.1016/j.renene.2023.119048, https://www.sciencedirect.com/science/article/pii/S096014812300962X.
[76] S.K. Vishnu, R. Senthil, Experimental performance and economic analysis of finned solar receiver for parabolic dish solar collector, Heliyon 9 (2023) e21236, https://doi.org/10.1016/j.heliyon.2023.e21236
[77] M. Lubkoll, D.J. Erasmus, T.M. Harms, T. von Backström, D.G. Kröger, Performance characteristics of the spiky central receiver air pre-heater (scrap), Sol. Energy 201 (2020) 773–786, https://doi.org/10.1016/j.solener.2020.03.027, https://www.sciencedirect.com/science/article/pii/S0038092X20302589.
[78] V. Thirunavukkarasu, M. Cheralathan, Experimental study on heat losses from external type receiver of a solar parabolic dish collector, IOP Conf. Ser. Mater. Sci. Eng. 402 (1) (2018) 012196, https://doi.org/10.1088/1757-899X/402/1/012196, https://dx.doi.org/10.1088/1757-899X/402/1/012196.
[79] S.-Y. Yang, R. Jiang, Z.-D. Cheng, X.-Z. Zhang, Y.-L. He, Experimental and numerical study on steady-state thermal performance of a kilowatt-scale chloride salt receiver prototype for the next-generation solar power tower, Energy Convers. Manag. 348 (2026) 120601, https://doi.org/10.1016/j.enconman.2025.120601, https://www.sciencedirect.com/science/article/pii/S0196890425011252.
[80] Freepik, Freepik — free vectors, stock photos & psd, https://www.freepik.com/ (Accessed: 27 October 2025).
[81] Vecteezy, Vecteezy — free vector art, stock photos & videos, https://www.vecteezy.com/ (Accessed: 27 October 2025).
[82] K. Ye, Q. Li, Y. Zhang, Y. Qiu, B. Liu, An efficient receiver tube enhanced by a solar transparent aerogel for solar power tower, Energy 261 (2022) 125313, https://doi.org/10.1016/j.energy.2022.125313, https://www.sciencedirect.com/science/article/pii/S0360544222021971.
[83] W.-Q. Wang, Y.-L. He, R. Jiang, A multi-scale solar receiver with peak receiver efficiency over 90% at 720 °C for the next-generation solar power tower, Renew. Energy 200 (2022) 714–723, https://doi.org/10.1016/j.renene.2022.09.122, https://www.sciencedirect.com/science/article/pii/S0960148122014811.
[84] M.J. Montes, R. Guédez, D. D'Souza, J.I. Linares, J. González-Aguilar, M. Romero, Proposal of a new design of central solar receiver for pressurised gases and supercritical fluids, Int. J. Therm. Sci. 194 (2023) 108586, https://doi.org/10.1016/j.ijthermalsci.2023.108586, https://www.sciencedirect.com/science/article/pii/S1290072923004477.
[85] A. Schmitt, F. Dinter, C. Reichel, Computational fluid dynamics study to reduce heat losses at the receiver of a solar tower plant, Sol. Energy 190 (2019) 286–300, https://doi.org/10.1016/j.solener.2019.07.079, https://www.sciencedirect.com/science/article/pii/S0038092X19307509.
[86] Q. Wang, Y. Yao, M. Hu, J. Cao, Y. Qiu, H. Yang, An air curtain surrounding the solar tower receiver for effective reduction of convective heat loss, Sustain. Cities Soc. 71 (2021) 103007, https://doi.org/10.1016/j.scs.2021.103007, https://www.sciencedirect.com/science/article/pii/S2210670721002924.
[87] W.-Q. Wang, Y. Qiu, M.-J. Li, Y.-L. He, Z.-D. Cheng, Coupled optical and thermal performance of a fin-like molten salt receiver for the next-generation solar power tower, Appl. Energy 272 (2020) 115079, https://doi.org/10.1016/j.apenergy.2020.115079, https://www.sciencedirect.com/science/article/pii/S0306261920305912.
[88] R. Mondal, J.F. Torres, G. Hughes, J. Pye, Air curtains for reduction of natural convection heat loss from a heated plate: A numerical investigation, Int. J. Heat Mass Transf. 189 (2022) 122709, https://doi.org/10.1016/j.ijheatmasstransfer.2022.122709, https://www.sciencedirect.com/science/article/pii/S0017931022001910.
[89] R. Mondal, J.F. Torres, G. Hughes, J. Pye, Optimal configuration of oblique air curtains for heat loss suppression from vertical solar-thermal receiver surfaces, Appl. Therm. Eng. 236 (2024) 121747, https://doi.org/10.1016/j.applthermaleng.2023.121747, https://www.sciencedirect.com/science/article/pii/S1359431123017763.
[90] Y. Wang, J. Pye, The peak flux constraints on bladed receiver performance in high-temperature molten salt concentrating solar power systems, in: Proceedings of 2016 Asia-Pacific Solar Research Conference, Australian National University in Canberra, Australia, 2016, https://apvi.org.au/solar-research-conference/wp-content/uploads/2017/11/Y-Wang-and-J-Pye.pdf.
[91] Y. Wang, C.-A. Asselineau, J. Coventry, J. Pye, Optical performance of bladed receivers for CSP systems, in: Energy Sustainability, vol. 1, 2016, p. V001T04A026. https://doi.org/10.1115/ES2016-59693
[92] F. Ghanadi, J.F. Torres, M. Arjomandi, J. Pye, Flow structure and convective heat transfer in a bladed structure under wind conditions, Int. J. Heat Fluid Flow 85 (2020) 108676, https://doi.org/10.1016/j.ijheatfluidflow.2020.108676, https://www.sciencedirect.com/science/article/pii/S0142727X20301028.
[93] J.F. Torres, F. Ghanadi, Y. Wang, M. Arjomandi, J. Pye, Mixed convection and radiation from an isothermal bladed structure, Int. J. Heat Mass Transf. 147 (2020) 118906, https://doi.org/10.1016/j.ijheatmasstransfer.2019.118906, https://www.sciencedirect.com/science/article/pii/S001793101835628X.
[94] R. Senthil, Effect of charging of phase change material in vertical and horizontal rectangular enclosures in a concentrated solar receiver, Case Stud. Therm. Eng. 21 (2020) 100653, https://doi.org/10.1016/j.csite.2020.100653, https://www.sciencedirect.com/science/article/pii/S2214157X20301799.
[95] T.N. Nallaperumal, R.K. Sellapandiyan, S.K. Vishnu, R. Senthil, Numerical and experimental analysis of a cross-finned solar receiver for parabolic dish collectors, Appl. Therm. Eng. 248 (2024) 123329, https://doi.org/10.1016/j.applthermaleng.2024.123329, https://www.sciencedirect.com/science/article/pii/S1359431124009979.
[96] R.D. Jilte, J.K. Nayak, S.B. Kedare, Experimental investigation on heat losses from differentially heated cylindrical cavity receiver used in paraboloid concentrator, J. Sol. Energy Eng. 139 (3) (2017) 031013, https://doi.org/10.1115/1.4036255, https://asmedigitalcollection.asme.org/solarenergyengineering/article-pdf/139/3/031013/6330093/sol_139_03_031013.pdf.
[97] A.M. Clausing, L.D. Lister, J.M. Waldvogel, Combined convection from isothermal cubical cavities with a variety of side-facing apertures, Int. J. Heat Mass Transf. 32 (8) (1989) 1561–1566, https://doi.org/10.1016/0017-9310(89)90077-X, https://www.sciencedirect.com/science/article/pii/001793108990077X.
[98] M. Prakash, Numerical study of natural convection heat loss from cylindrical solar cavity receivers, Int. Sch. Res. Not. 2014 (1) (2014) 104686, https://doi.org/10.1155/2014/104686, https://onlinelibrary.wiley.com/doi/pdf/10.1155/2014/104686.
[99] J. Fang, N. Tu, J. Wei, Effects of absorber emissivity on thermal performance of a solar cavity receiver, Adv. Condens. Matter Phys. 2014 (1) (2014) 564639, https://doi.org/10.1155/2014/564639, https://onlinelibrary.wiley.com/doi/pdf/10.1155/2014/564639.
[100] S. Sharma, S.K. Saha, Development of scaling laws for prototyping and heat loss correlations for upward facing cylindrical helical coil and conical spiral coil receivers, Int. J. Heat Mass Transf. 190 (2022) 122773, https://doi.org/10.1016/j.ijheatmasstransfer.2022.122773, https://www.sciencedirect.com/science/article/pii/S0017931022002551.
[101] P. Mandal, A. Rajan, K.S. Reddy, Optical and thermal investigation of hyperbolic cavity receiver with secondary reflector for solar parabolic dish collector, Therm. Sci. Eng. Prog. 47 (2024) 102350, https://doi.org/10.1016/j.tsep.2023.102350, https://www.sciencedirect.com/science/article/pii/S2451904923007035.
[102] K.H. Kumar, M. Karmakar, B. Mondal, Numerical analysis of convective heat loss from a cylindrical–hemispherical receiver using a glass cover and an air curtain, Heat Transf. 53 (4) (2024) 2039–2061, https://doi.org/10.1002/htj.23025, https://onlinelibrary.wiley.com/doi/pdf/10.1002/htj.23025.
[103] R. Flesch, H. Stadler, R. Uhlig, B. Hoffschmidt, On the influence of wind on cavity receivers for solar power towers: An experimental analysis, Appl. Therm. Eng. 87 (2015) 724–735, https://doi.org/10.1016/j.applthermaleng.2015.05.059, https://www.sciencedirect.com/science/article/pii/S1359431115005153.
[104] R. Flesch, H. Stadler, R. Uhlig, R. Pitz-Paal, Numerical analysis of the influence of inclination angle and wind on the heat losses of cavity receivers for solar thermal power towers, Sol. Energy 110 (2014) 427–437, https://doi.org/10.1016/j.solener.2014.09.045, https://www.sciencedirect.com/science/article/pii/S0038092X14004873.
[105] Z.-G. Shen, S.-Y. Wu, L. Xiao, Numerical study of wind effects on combined convective heat loss from an upward-facing cylindrical cavity, Sol. Energy 132 (2016) 294–309, https://doi.org/10.1016/j.solener.2016.03.021, https://www.sciencedirect.com/science/article/pii/S0038092X16002085.
[106] L. Xiao, S. He, Z.-G. Shen, S.-Y. Wu, Z.-L. Chen, Wind-induced convective heat loss of cylindrical receiver considering the effect of dish concentrator,

Renew. Energy 182 (2022) 900–912, https://doi.org/10.1016/j.renene.2021.10.077, https://www.sciencedirect.com/science/article/pii/S0960148121015366.
[107] S.-Y. Wu, Z.-G. Shen, L. Xiao, D.-L. Li, Experimental study on combined convective heat loss of a fully open cylindrical cavity under wind conditions, Int. J. Heat Mass Transf. 83 (2015) 509–521, https://doi.org/10.1016/j.ijheatmasstransfer.2014.12.029, https://www.sciencedirect.com/science/article/pii/S0017931014011193.
[108] K.L. Lee, A. Chinnici, M. Jafarian, M. Arjomandi, B. Dally, G. Nathan, The influence of wind speed, aperture ratio and tilt angle on the heat losses from a finely controlled heated cavity for a solar receiver, Renew. Energy 143 (2019) 1544–1553, https://doi.org/10.1016/j.renene.2019.05.015, https://www.sciencedirect.com/science/article/pii/S0960148119306676.
[109] T. Yazdanipour, F. Shahraki, D.M. Kalhori, Experimental analysis of free convection heat loss in a bicylindrical cavity receiver, Therm. Sci. Eng. Prog. 20 (2020) 100663, https://doi.org/10.1016/j.tsep.2020.100663, https://www.sciencedirect.com/science/article/pii/S2451904920301839.
[110] W. Wu, L. Amsbeck, R. Buck, N. Waibel, P. Langner, R. Pitz-Paal, On the influence of rotation on thermal convection in a rotating cavity for solar receiver applications, Appl. Therm. Eng. 70 (1) (2014) 694–704, https://doi.org/10.1016/j.applthermaleng.2014.03.059, https://www.sciencedirect.com/science/article/pii/S1359431114002385.
[111] C. Zou, Y. Zhang, H. Feng, Q. Falcoz, P. Neveu, W. Gao, C. Zhang, Effects of geometric parameters on thermal performance for a cylindrical solar receiver using a 3D numerical model, Energy Convers. Manag. 149 (2017) 293–302, https://doi.org/10.1016/j.enconman.2017.06.088, https://www.sciencedirect.com/science/article/pii/S0196890417306349.
[112] E. Abbasi-Shavazi, J.F. Torres, G. Hughes, J. Pye, Experimental correlation of natural convection losses from a scale-model solar cavity receiver with non-isothermal surface temperature distribution, Sol. Energy 198 (2020) 355–375, https://doi.org/10.1016/j.solener.2020.01.023, https://www.sciencedirect.com/science/article/pii/S0038092X20300232.
[113] J.K. Swanepoel, W.G. le Roux, C. Roosendaal, J. Buys, Convection heat loss analysis of a wind-skirted open-cavity tubular receiver for a solar-dish brayton cycle, Sol. Energy 287 (2025) 113197, https://doi.org/10.1016/j.solener.2024.113197, https://www.sciencedirect.com/science/article/pii/S0038092X24008922.
[114] M.A. Bashir, H.M. Ali, Numerical assessment of the effect of tube geometries on the performance of phase change material (PCM) integrated solar receiver for dish-micro gas turbine systems, J. Energy Storage 68 (2023) 107725, https://doi.org/10.1016/j.est.2023.107725, https://www.sciencedirect.com/science/article/pii/S2352152X23011222.
[115] Y. Zhi, S. shuai Liu, B. Yang, X. hui Yu, Analysis of the thermal performance of parabolic solar dish collector using mcrt-fvm coupled optical-thermal model, Energy 322 (2025) 135579, https://doi.org/10.1016/j.energy.2025.135579, https://www.sciencedirect.com/science/article/pii/S0360544225012216.
[116] K.L. Lee, M. Jafarian, F. Ghanadi, M. Arjomandi, G.J. Nathan, An investigation into the effect of aspect ratio on the heat loss from a solar cavity receiver, Sol. Energy 149 (2017) 20–31, https://doi.org/10.1016/j.solener.2017.03.089, https://www.sciencedirect.com/science/article/pii/S0038092X17302803.
[117] K.L. Lee, A. Chinnici, M. Jafarian, M. Arjomandi, B. Dally, G. Nathan, Experimental investigation of the effects of wind speed and yaw angle on heat losses from a heated cavity, Sol. Energy 165 (2018) 178–188, https://doi.org/10.1016/j.solener.2018.03.023, https://www.sciencedirect.com/science/article/pii/S0038092X18302342.
[118] S. Siegrist, H. Stadler, B. Hoffschmidt, Wind tunnel measurements of forced convective heat loss from multi-megawatt cavities of solar central receiver systems, Sol. Energy 169 (2018) 607–615, https://doi.org/10.1016/j.solener.2018.04.029, https://www.sciencedirect.com/science/article/pii/S0038092X18303748.
[119] A. Msaddak, E. Sediki, M. Ben Salah, Assessment of thermal heat loss from solar cavity receiver with lattice boltzmann method, Sol. Energy 173 (2018) 1115–1125, https://doi.org/10.1016/j.solener.2018.08.059, https://www.sciencedirect.com/science/article/pii/S0038092X18308302.
[120] K.J. Craig, M. Slootweg, W.G. Le Roux, T.M. Wolff, J.P. Meyer, Using CFD and ray tracing to estimate the heat losses of a tubular cavity dish receiver for different inclination angles, Sol. Energy 211 (2020) 1137–1158, https://doi.org/10.1016/j.solener.2020.10.054, https://www.sciencedirect.com/science/article/pii/S0038092X20311130.
[121] T. Hussain, M.D. Islam, I. Kubo, T. Watanabe, Study of heat transfer through a cavity receiver for a solar powered advanced stirling engine generator, Appl. Therm. Eng. 104 (2016) 751–757, https://doi.org/10.1016/j.applthermaleng.2016.05.108, https://www.sciencedirect.com/science/article/pii/S135943111630775X.
[122] S.-Y. Wu, J.-Y. Guan, L. Xiao, Z.-G. Shen, L.-H. Xu, Experimental investigation on heat loss of a fully open cylindrical cavity with different boundary conditions, Exp. Therm. Fluid Sci. 45 (2013) 92–101, https://doi.org/10.1016/j.expthermflusci.2012.10.010, https://www.sciencedirect.com/science/article/pii/S0894177712002804.
[123] L. Xiao, S.-Y. Wu, Y.-R. Li, Numerical study on combined free-forced convection heat loss of solar cavity receiver under wind environments, Int. J. Therm. Sci. 60 (2012) 182–194, https://doi.org/10.1016/j.ijthermalsci.2012.05.008, https://www.sciencedirect.com/science/article/pii/S1290072912001585.
[124] K.L. Lee, A. Chinnici, M. Jafarian, M. Arjomandi, B. Dally, G. Nathan, The influence of wall temperature distribution on the mixed convective losses from a heated cavity, Appl. Therm. Eng. 155 (2019) 157–165, https://doi.org/10.1016/j.applthermaleng.2019.03.052, https://www.sciencedirect.com/science/article/pii/S1359431118360435.
[125] K. Wang, X.-X. Liu, Z.-G. Shen, H.-H. Duan, Q.-S. Liu, Y.-S. Wu, A numerical study on the natural convective heat loss of an isothermal upward-facing cylindrical cavity, Appl. Therm. Eng. 213 (2022) 118763, https://doi.org/10.1016/j.applthermaleng.2022.118763, https://www.sciencedirect.com/science/article/pii/S1359431122007050.
[126] E. Abbasi-Shavazi, G.O. Hughes, J.D. Pye, Investigation of heat loss from a solar cavity receiver, Energy Procedia 69 (2015) 269–278, International Conference on Concentrating Solar Power and Chemical Energy Systems, SolarPACES 2014. https://doi.org/10.1016/j.egypro.2015.03.031, https://www.sciencedirect.com/science/article/pii/S1876610215003379.
[127] J.-Q. Li, J.-T. Kwon, S.-J. Jang, The power and efficiency analyses of the cylindrical cavity receiver on the solar stirling engine, Energies 13 (21) (2020), https://doi.org/10.3390/en13215798, https://www.mdpi.com/1996-1073/13/21/5798.
[128] R. Sinha, N.P. Gulhane, Numerical study of radiation heat loss from solar cavity receiver of parabolic dish collector, Numer. Heat Transf. a Appl. 77 (7) (2020) 743–759, https://doi.org/10.1080/10407782.2020.1714366
[129] J.K. Yuan, C.K. Ho, J.M. Christian, Numerical simulation of natural convection in solar cavity receivers, J. Sol. Energy Eng. 137 (3) (2015) 031004, https://doi.org/10.1115/1.4029106, https://asmedigitalcollection.asme.org/solarenergyengineering/article-pdf/137/3/031004/6327233/sol_137_03_031004.pdf.
[130] L. Xiao, F.-W. Guo, S.-Y. Wu, Z.-L. Chen, A comprehensive simulation on optical and thermal performance of a cylindrical cavity receiver in a parabolic dish collector system, Renew. Energy 145 (2020) 878–892, https://doi.org/10.1016/j.renene.2019.06.068, https://www.sciencedirect.com/science/article/pii/S0960148119308961.
[131] A. Chinnici, Z.F. Tian, J.H. Lim, G.J. Nathan, B.B. Dally, Comparison of system performance in a hybrid solar receiver combustor operating with MILD and conventional combustion. Part I: Solar-only and combustion-only employing conventional combustion, Sol. Energy 147 (2017) 489–503, https://doi.org/10.1016/j.solener.2017.02.055, https://www.sciencedirect.com/science/article/pii/S0038092X1730155X.
[132] A. Chinnici, G.J. Nathan, B.B. Dally, Experimental demonstration of the hybrid solar receiver combustor, Appl. Energy 224 (2018) 426–437, https://doi.org/10.1016/j.apenergy.2018.05.021, https://www.sciencedirect.com/science/article/pii/S030626191830713X.
[133] C. Zou, Y. Zhang, Q. Falcoz, P. Neveu, C. Zhang, W. Shu, S. Huang, Design and optimization of a high-temperature cavity receiver for a solar energy cascade utilization system, Renew. Energy 103 (2017) 478–489, https://doi.org/10.1016/j.renene.2016.11.044, https://www.sciencedirect.com/science/article/pii/S0960148116310138.
[134] D. Azzouzi, B. Boumeddane, A. Abene, Experimental and analytical thermal analysis of cylindrical cavity receiver for solar dish, Renew. Energy 106 (2017) 111–121, https://doi.org/10.1016/j.renene.2016.12.102, https://www.sciencedirect.com/science/article/pii/S0960148116310515.
[135] Z. Yanping, C. Yuxuan, Z. Chongzhe, X. Hu, Q. Falcoz, P. Neveu, Z. Cheng, H. Xiaohong, Experimental investigation on heat-transfer characteristics of a cylindrical cavity receiver with pressurized air in helical pipe, Renew. Energy 163 (2021) 320–330, https://doi.org/10.1016/j.renene.2020.09.009, https://www.sciencedirect.com/science/article/pii/S0960148120314178.
[136] C. Ophoff, N. Ozalp, D. Moens, Experimental performance comparison and optical characteristics of aperture mechanisms for solar cavity receivers, Sol. Energy 188 (2019) 66–82, https://doi.org/10.1016/j.solener.2019.05.079, https://www.sciencedirect.com/science/article/pii/S0038092X19305614.
[137] J.K. Swanepoel, W.G. le Roux, A.S. Lexmond, J.P. Meyer, Helically coiled solar cavity receiver for micro-scale direct steam generation, Appl. Therm. Eng. 185 (2021) 116427, https://doi.org/10.1016/j.applthermaleng.2020.116427, https://www.sciencedirect.com/science/article/pii/S1359431120339053.
[138] L.S. Mendoza Castellanos, G.E. Carrillo Caballero, V.R. Melian Cobas, E.E. Silva Lora, A.M. Martinez Reyes, Mathematical modeling of the geometrical sizing and thermal performance of a dish/stirling system for power generation, Renew. Energy 107 (2017) 23–35, https://doi.org/10.1016/j.renene.2017.01.020, https://www.sciencedirect.com/science/article/pii/S0960148117300204.
[139] B. Guene Lougou, D. Han, H. Zhang, B. Jiang, J. Anees, C. Ahouannou, J. Zhao, Y. Shuai, Numerical and experimental analysis of reactor optimum design and solar thermal-chemical energy conversion for multidisciplinary applications, Energy Convers. Manag. 213 (2020) 112870, https://doi.org/10.1016/j.enconman.2020.112870, https://www.sciencedirect.com/science/article/pii/S0196890420304088.
[140] L. Xiao, S. He, S.-Y. Wu, Z.-L. Chen, Optical-thermal conversion characteristics of cylindrical receiver with built-in helically coiled tubes, Sustain. Energy Technol. Assess. 37 (2020) 100626, https://doi.org/10.1016/j.seta.2019.100626, https://www.sciencedirect.com/science/article/pii/S2213138819306290.
[141] G.E. Carrillo Caballero, L.S. Mendoza, A.M. Martinez, E.E. Silva, V.R. Melian, O.J. Venturini, O.A. del Olmo, Optimization of a dish stirling system working with dir-type receiver using multi-objective techniques, Appl. Energy 204 (2017) 271–286, https://doi.org/10.1016/j.apenergy.2017.07.053, https://www.sciencedirect.com/science/article/pii/S030626191730925X.
[142] C. Zou, H. Feng, Y. Zhang, et al., Geometric optimization model for the solar cavity receiver with helical pipe at different solar radiation, Front. Energy 13 (2019) 284–295, https://doi.org/10.1007/s11708-019-0613-3
[143] Z. Wang, K. Wu, T. Wang, et al., Numerical study of convective and radiation heat transfer characteristics in an upward-facing cylindrical cavity under backside windy condition, J. Therm. Sci. 30 (2021) 302–312, https://doi.org/10.1007/s11630-020-1309-z

[144] D. Malwad, V. Tungikar, Experimental performance analysis of an improved receiver for scheffler solar concentrator, SN Appl. Sci. 2 (2020) 1992, https://doi.org/10.1007/s42452-020-03848-y
[145] K. Qiu, L. Yan, M. Ni, C. Wang, G. Xiao, Z. Luo, K. Cen, Simulation and experimental study of an air tube-cavity solar receiver, Energy Convers. Manag. 103 (2015) 847–858, https://doi.org/10.1016/j.enconman.2015.07.013, https://www.sciencedirect.com/science/article/pii/S0196890415006640.
[146] R. Loni, E. Askari Asli-Ardeh, B. Ghobadian, A.B. Kasaeian, E. Bellos, Thermal performance comparison between Al_2O_3/oil and SiO_2/oil nanofluids in cylindrical cavity receiver based on experimental study, Renew. Energy 129 (2018) 652–665, https://doi.org/10.1016/j.renene.2018.06.029, https://www.sciencedirect.com/science/article/pii/S0960148118306529.
[147] K.S. Reddy, T.S. Vikram, G. Veershetty, Combined heat loss analysis of solar parabolic dish – modified cavity receiver for superheated steam generation, Sol. Energy 121 (2015) 78–93, iSES Solar World Congress 2013 (SWC2013) Special Issue. https://doi.org/10.1016/j.solener.2015.04.028, https://www.sciencedirect.com/science/article/pii/S0038092X15002169.
[148] Y. Li, G. Liu, Z. Rao, S. Liao, Field synergy principle analysis for reducing natural convection heat loss of a solar cavity receiver, Renew. Energy 75 (2015) 257–265, https://doi.org/10.1016/j.renene.2014.09.055, https://www.sciencedirect.com/science/article/pii/S096014811400620X.
[149] T.S. Vikram, K.S. Reddy, Investigation of convective and radiative heat losses from modified cavity based solar dish steam generator using ann, Int. J. Therm. Sci. 87 (2015) 19–30, https://doi.org/10.1016/j.ijthermalsci.2014.08.005, https://www.sciencedirect.com/science/article/pii/S1290072914002300.
[150] K.S. Reddy, S.K. Natarajan, G. Veershetty, Experimental performance investigation of modified cavity receiver with fuzzy focal solar dish concentrator, Renew. Energy 74 (2015) 148–157, https://doi.org/10.1016/j.renene.2014.07.058, https://www.sciencedirect.com/science/article/pii/S096014811400456X.
[151] K.S. Reddy, G. Veershetty, T. Srihari Vikram, Effect of wind speed and direction on convective heat losses from solar parabolic dish modified cavity receiver, Sol. Energy 131 (2016) 183–198, https://doi.org/10.1016/j.solener.2016.02.039, https://www.sciencedirect.com/science/article/pii/S0038092X16001481.
[152] R. Loni, E. Askari Asli-Ardeh, B. Ghobadian, A.B. Kasaeian, S. Gorjian, Numerical and experimental investigation of wind effect on a hemispherical cavity receiver, Appl. Therm. Eng. 126 (2017) 179–193, https://doi.org/10.1016/j.applthermaleng.2017.07.097, https://www.sciencedirect.com/science/article/pii/S1359431117307603.
[153] V.C. Shewale, P.R. Dongarwar, R.R. Gawande, Heat loss investigation from spherical cavity receiver of solar concentrator, J. Mech. Sci. Technol. 30 (2016) 5233–5238, https://doi.org/10.1007/s12206-016-1040-6
[154] Y. Tan, L. Zhao, J. Bao, Q. Liu, Experimental investigation on heat loss of semi-spherical cavity receiver, Energy Convers. Manag. 87 (2014) 576–583, https://doi.org/10.1016/j.enconman.2014.06.080, https://www.sciencedirect.com/science/article/pii/S0196890414006050.
[155] S.B. Bopche, S. Kumar, Experimental investigations on thermal performance characteristics of a solar cavity receiver, International Journal of Energy Environmental Engineering 10 (2019) 463–481, https://doi.org/10.1007/s40095-019-00321-4
[156] S.Y. Khan, M. Uzair, U. Allauddin, Coupled optical-thermal performance enhancement of solar parabolic dish system using a hemiellipsoidal tubular receiver, Renew. Energy 256 (2026) 124434, https://doi.org/10.1016/j.renene.2025.124434, https://www.sciencedirect.com/science/article/pii/S0960148125020981.
[157] M. Uzair, T.N. Anderson, R.J. Nates, Modeling of convective heat loss from a cavity receiver coupled to a dish concentrator, Sol. Energy 176 (2018) 496–505, https://doi.org/10.1016/j.solener.2018.10.060, https://www.sciencedirect.com/science/article/pii/S0038092X18310399.
[158] M. Uzair, T.N. Anderson, R.J. Nates, The impact of the parabolic dish concentrator on the wind induced heat loss from its receiver, Sol. Energy 151 (2017) 95–101, https://doi.org/10.1016/j.solener.2017.05.022, https://www.sciencedirect.com/science/article/pii/S0038092X17303997.
[159] Y. Zhang, H. Xiao, C. Zou, Q. Falcoz, P. Neveu, Combined optics and heat transfer numerical model of a solar conical receiver with built-in helical pipe, Energy 193 (2020) 116775, https://doi.org/10.1016/j.energy.2019.116775, https://www.sciencedirect.com/science/article/pii/S0360544219324703.
[160] X. Li, Y.J. Dai, R.Z. Wang, Performance investigation on solar thermal conversion of a conical cavity receiver employing a beam-down solar tower concentrator, Sol. Energy 114 (2015) 134–151, https://doi.org/10.1016/j.solener.2015.01.033, https://www.sciencedirect.com/science/article/pii/S0038092X1500047X.
[161] T. Venkatachalam, M. Cheralathan, Effect of aspect ratio on thermal performance of cavity receiver for solar parabolic dish concentrator: An experimental study, Renew. Energy 139 (2019) 573–581, https://doi.org/10.1016/j.renene.2019.02.102, https://www.sciencedirect.com/science/article/pii/S0960148119302563.
[162] M.A. Bashir, A. Giovannelli, H.M. Ali, Design of high-temperature solar receiver integrated with short-term thermal storage for dish-micro gas turbine systems, Sol. Energy 190 (2019) 156–166, https://doi.org/10.1016/j.solener.2019.07.077, https://www.sciencedirect.com/science/article/pii/S0038092X19307480.
[163] M.A. Bashir, H.M. Ali, Design and analysis of PCM integrated solar receiver with double-helical tube structure, J. Energy Storage 84 (2024) 110872, https://doi.org/10.1016/j.est.2024.110872, https://www.sciencedirect.com/science/article/pii/S2352152X24004560.
[164] A.A. Sagade, Comparative experimental analysis of the effect of convective heat losses on the performance of parabolic dish water heater, Int. J. Sustain. Eng. 6 (3) (2013) 258–266, https://doi.org/10.1080/19397038.2012.691566
[165] K.K. Murugavel, M. Vivekanandan, E. Tamil Kumaran, R. Shanmuga Raj, V. Shriram, M. Sankara Pandian, Comparative study on convection loss of different shape solar dish collector cavity receivers at different positions using CFD, Mater. Today Proc. 37 (2021) 3091–3095, International Conference on Newer Trends and Innovation in Mechanical Engineering: Materials Science. https://doi.org/10.1016/j.matpr.2020.09.018, https://www.sciencedirect.com/science/article/pii/S2214785320366980.
[166] N. Tu, J. Wei, J. Fang, Numerical study on thermal performance of a solar cavity receiver with different depths, Appl. Therm. Eng. 72 (1) (2014) 20–28, aS-CHT2013. https://doi.org/10.1016/j.applthermaleng.2014.01.017, https://www.sciencedirect.com/science/article/pii/S1359431114000234.
[167] T. Hu, P. Jia, Y. Wang, Y. Hao, Numerical simulation on convective thermal loss of a cavity receiver in a solar tower power plant, Sol. Energy 150 (2017) 202–211, https://doi.org/10.1016/j.solener.2017.04.008, https://www.sciencedirect.com/science/article/pii/S0038092X17302918.
[168] Q. Deng, X. Xiao, Y. Hao, Q. Wang, T. Hu, Y. Wang, Heat transfer performance evaluation of a large-size cavity receiver in the solar power tower plant based on angle factors, Sol. Energy 148 (2017) 78–86, https://doi.org/10.1016/j.solener.2017.03.067, https://www.sciencedirect.com/science/article/pii/S0038092X17302396.
[169] M. Slootweg, K.J. Craig, J.P. Meyer, A computational approach to simulate the optical and thermal performance of a novel complex geometry solar tower molten salt cavity receiver, Sol. Energy 187 (2019) 13–29, https://doi.org/10.1016/j.solener.2019.05.003, https://www.sciencedirect.com/science/article/pii/S0038092X19304487.
[170] J. Fang, N. Tu, J. Wei, X. Du, Effects of surface optical and radiative properties on the thermal performance of a solar cavity receiver, Sol. Energy 171 (2018) 157–170, https://doi.org/10.1016/j.solener.2018.06.075, https://www.sciencedirect.com/science/article/pii/S0038092X18306261.
[171] N. Tu, J. Fang, Z. Wan, J. Wei, Effects of the superheater layout on the thermal performance of a central cavity receiver, Appl. Therm. Eng. 158 (2019) 113784, https://doi.org/10.1016/j.applthermaleng.2019.113784, https://www.sciencedirect.com/science/article/pii/S1359431118357958.
[172] L. Zhang, J. Fang, J. Wei, G. Yang, Numerical investigation on the thermal performance of molten salt cavity receivers with different structures, Appl. Energy 204 (2017) 966–978, https://doi.org/10.1016/j.apenergy.2017.03.114, https://www.sciencedirect.com/science/article/pii/S0306261917303550.
[173] N. Tu, J. Wei, J. Fang, Numerical investigation on uniformity of heat flux for semi-gray surfaces inside a solar cavity receiver, Sol. Energy 112 (2015) 128–143, https://doi.org/10.1016/j.solener.2014.11.028, https://www.sciencedirect.com/science/article/pii/S0038092X14005726.
[174] J.I. Linares, M.J. Montes, A. Cantizano, C. Sánchez, A novel supercritical Co2 recompression brayton power cycle for power tower concentrating solar plants, Appl. Energy 263 (2020) 114644, https://doi.org/10.1016/j.apenergy.2020.114644, https://www.sciencedirect.com/science/article/pii/S0306261920301562.
[175] A.P. Ortiz, J.F.H. Palafox, C.A.E. Gasca, Numerical study of heat transfer losses by mixed convection and surface thermal radiation in an open cavity receiver for a solar tower system, Energy Procedia 57 (2014) 467–476, 2013 ISES Solar World Congress. https://doi.org/10.1016/j.egypro.2014.10.200, https://www.sciencedirect.com/science/article/pii/S1876610214015677.
[176] Z. Chang, X. Li, C. Xu, C. Chang, Z. Wang, Numerical simulation on the thermal performance of a solar molten salt cavity receiver, Renew. Energy 69 (2014) 324–335, https://doi.org/10.1016/j.renene.2014.03.044, https://www.sciencedirect.com/science/article/pii/S0960148114002080.
[177] Y. Luo, X. Du, D. Wen, Novel design of central dual-receiver for solar power tower, Appl. Therm. Eng. 91 (2015) 1071–1081, https://doi.org/10.1016/j.applthermaleng.2015.08.074, https://www.sciencedirect.com/science/article/pii/S1359431115008704.
[178] O. Singh, S.B. Kedare, S. Singh, Analysis of fluid flow and heat transfer in the novel liquid volumetric plated cavity receiver, Sol. Energy 231 (2022) 420–432, https://doi.org/10.1016/j.solener.2021.11.059, https://www.sciencedirect.com/science/article/pii/S0038092X21010197.
[179] J. Martinek, R. Viger, A.W. Weimer, Transient simulation of a tubular packed bed solar receiver for hydrogen generation via metal oxide thermochemical cycles, Sol. Energy 105 (2014) 613–631, https://doi.org/10.1016/j.solener.2014.04.022, https://www.sciencedirect.com/science/article/pii/S0038092X14002187.
[180] E. Alipourtarzanagh, A. Chinnici, G.J. Nathan, B.B. Dally, Experimental insights into the mechanism of heat losses from a cylindrical solar cavity receiver equipped with an air curtain, Sol. Energy 201 (2020) 314–322, https://doi.org/10.1016/j.solener.2020.03.004, https://www.sciencedirect.com/science/article/pii/S0038092X20302358.
[181] Y.N. Nandanwar, P.V. Walke, Performance analysis of phase change material (pcm) integrated conical cavity receiver in solar parabolic dish collector, Energy Storage Sav. 4 (2) (2025) 166–178, https://doi.org/10.1016/j.enss.2024.12.001, https://www.sciencedirect.com/science/article/pii/S2772683525000020.
[182] X. Li, R. Li, H. Chang, L. Zeng, Z. Xi, Y. Li, Numerical simulation of a cavity receiver enhanced with transparent aerogel for parabolic dish solar power generation, Energy 246 (2022) 123358, https://doi.org/10.1016/j.energy.2022.123358, https://www.sciencedirect.com/science/article/pii/S0360544222002614.
[183] X. Na, Y. Yao, C. Zhao, J. Du, Heat loss reduction approach in cavity receiver design based on performance investigation of a novel positive conical scheme, Energies 15 (3) (2022), https://doi.org/10.3390/en15030784, https://www.mdpi.com/1996-1073/15/3/784.
[184] H. Mobasheri-Shiri, T. Yazdanipour, K. Razzaghi, Convective heat loss from a modified solar cavity receiver with vertical plate fins: An experimental assessment, Heat Transf. 53 (7) (2024) 3525–3546, https://doi.org/10.1002/htj.23100

[185] L.C. Ngo, T. Bello-Ochende, J.P. Meyer, Three-dimensional analysis and numerical optimization of combined natural convection and radiation heat loss in solar cavity receiver with plate fins insert, Energy Convers. Manag. 101 (2015) 757–766, https://doi.org/10.1016/j.enconman.2015.05.061, https://www.sciencedirect.com/science/article/pii/S0196890415005269.
[186] L.C. Ngo, T. Bello-Ochende, J.P. Meyer, Numerical modelling and optimisation of natural convection heat loss suppression in a solar cavity receiver with plate fins, Renew. Energy 74 (2015) 95–105, https://doi.org/10.1016/j.renene.2014.07.047, https://www.sciencedirect.com/science/article/pii/S0960148114004455.
[187] S. Bopche, K. Rana, V. Kumar, Performance improvement of a modified cavity receiver for parabolic dish concentrator at medium and high heat concentration, Sol. Energy 209 (2020) 57–78, https://doi.org/10.1016/j.solener.2020.08.089, https://www.sciencedirect.com/science/article/pii/S0038092X20309294.
[188] R. Uhlig, R. Flesch, B. Gobereit, S. Giuliano, P. Liedke, Strategies enhancing efficiency of cavity receivers, Energy Procedia 49 (2014) 538–550, Proceedings of the SolarPACES 2013 International Conference. doi:https://doi.org/10.1016/j.egypro.2014.03.058, https://www.sciencedirect.com/science/article/pii/S1876610214005128.
[189] L. Xiao, X.-D. Cai, S.-Y. Wu, Experimental investigation on natural convective heat loss of cylindrical cavity with/without a quartz window, Int. J. Therm. Sci. 150 (2020) 106220, https://doi.org/10.1016/j.ijthermalsci.2019.106220, https://www.sciencedirect.com/science/article/pii/S129007291930777X.
[190] A.M. Daabo, A. Ahmad, S. Mahmoud, R.K. Al-Dadah, Parametric analysis of small scale cavity receiver with optimum shape for solar powered closed brayton cycle applications, Appl. Therm. Eng. 122 (2017) 626–641, https://doi.org/10.1016/j.applthermaleng.2017.03.093, https://www.sciencedirect.com/science/article/pii/S1359431117318689.
[191] S. Yang, J. Wang, P.D. Lund, S. Wang, C. Jiang, Reducing convective heat losses in solar dish cavity receivers through a modified air-curtain system, Sol. Energy 166 (2018) 50–58, https://doi.org/10.1016/j.solener.2018.03.027, https://www.sciencedirect.com/science/article/pii/S0038092X1830238X.
[192] E. Alipourtarzanagh, A. Chinnici, G.J. Nathan, B.B. Dally, Impact of flow blowing and suction strategies on the establishment of an aerodynamic barrier for solar cavity receivers, Appl. Therm. Eng. 180 (2020) 115841, https://doi.org/10.1016/j.applthermaleng.2020.115841, https://www.sciencedirect.com/science/article/pii/S1359431120333238.
[193] A. Cheilytko, P. Schwarzbözl, Reducing convective losses in a solar cavity receiver vocorec by creating a controlled vortex of returned air, Renew. Energy 230 (2024) 120898, https://doi.org/10.1016/j.renene.2024.120898, https://www.sciencedirect.com/science/article/pii/S0960148124009662.
[194] J. Fang, N. Tu, J.F. Torres, J. Wei, J.D. Pye, Numerical investigation of the natural convective heat loss of a solar central cavity receiver with air curtain, Appl. Therm. Eng. 152 (2019) 147–159, https://doi.org/10.1016/j.applthermaleng.2019.02.087, https://www.sciencedirect.com/science/article/pii/S1359431118314911.
[195] J.J. Zhang, J.D. Pye, G.O. Hughes, Active air flow control to reduce cavity receiver heat loss, in: ASME 2015 9th International Conference on Energy Sustainability collocated with the ASME 2015 Power Conference, the ASME 2015 13th International Conference on Fuel Cell Science, Engineering and Technology, and the ASME 2015 Nuclear Forum, vol. 1, 2015, p. V001T05A023. https://doi.org/10.1115/ES2015-49710
[196] S. Wang, C.-A. Asselineau, Y. Wang, J. Pye, J. Coventry, Performance enhancement of cavity receivers with spillage skirts and secondary reflectors in concentrated solar dish and tower systems, Sol. Energy 208 (2020) 708–727, https://doi.org/10.1016/j.solener.2020.08.008, https://www.sciencedirect.com/science/article/pii/S0038092X20308409.
[197] X. long Meng, X. lin Xia, S. de Zhang, N. Sellami, T. Mallick, Coupled heat transfer performance of a high temperature cup shaped porous absorber, Energy Convers. Manag. 110 (2016) 327–337, https://doi.org/10.1016/j.enconman.2015.12.034, https://www.sciencedirect.com/science/article/pii/S0196890415011371.
[198] Z. Wan, J. Wei, J. Su, M.A. Qaisrani, J. Fang, Y. Jin, Convective heat loss under windy conditions and effects of porous shroud for large scale cavity receiver, Sol. Energy 286 (2025) 113202, https://doi.org/10.1016/j.solener.2024.113202, https://www.sciencedirect.com/science/article/pii/S0038092X24008971.
[199] C. Fan, X. Zhang, W. Liu, S. Han, W. Xu, S. Tian, L. Han, Energy-efficient production of sustainable industrial process heat with a parabolic dish-conical cavity solar collector, J. Clean. Prod. 470 (2024) 143282, https://doi.org/10.1016/j.jclepro.2024.143282, https://www.sciencedirect.com/science/article/pii/S0959652624027318.
[200] A.S. Kopalakrishnaswami, S.K. Natarajan, Comparative study of modified conical cavity receiver with other receivers for solar paraboloidal dish collector system, Environ. Sci. Pollut. Res. 29 (2022) 7548–7558, https://doi.org/10.1007/s11356-021-16127-z
[201] K.E. Elfeky, Q. Wang, Techno-environ-economic assessment of photovoltaic and CSP with storage systems in china and Egypt under various climatic conditions, Renew. Energy 215 (2023) 118930, https://doi.org/10.1016/j.renene.2023.118930, https://www.sciencedirect.com/science/article/pii/S0960148123008364.
[202] A.B. Awan, M. Zubair, R.P. Praveen, A.R. Bhatti, Design and comparative analysis of photovoltaic and parabolic trough based CSP plants, Sol. Energy 183 (2019) 551–565, https://doi.org/10.1016/j.solener.2019.03.037, https://www.sciencedirect.com/science/article/pii/S0038092X19302658.
[203] A. Boretti, Cost and production of solar thermal and solar photovoltaics power plants in the united states, Renew. Energy Focus 26 (2018) 93–99, https://doi.org/10.1016/j.ref.2018.07.002, https://www.sciencedirect.com/science/article/pii/S1755008418300334.
[204] M. Mehos, C. Turchi, J. Jorgensen, P. Denholm, C.K. Ho, K.M. Armijo, On the path to sunshot: Advancing concentrating solar power technology, performance, and dispatchability, Tech. Rep. 1561032, Sandia National Lab, Albuquerque, NM, United States; National Renewable Energy Laboratory (NREL), Golden, CO, United States, 2016, https://doi.org/10.2172/1561032. https://www.osti.gov/biblio/1561032.
[205] P. Denholm, M. Mehos, Enabling greater penetration of solar power via the use of CSP with thermal energy storage, Tech. Rep. 1030440, National Renewable Energy Lab. (NREL), Golden, CO, United States, 2011, https://doi.org/10.2172/1030440. https://www.osti.gov/biblio/1030440.
[206] F. Schöniger, R. Thonig, G. Resch, J. Lilliestam, Making the sun shine at night: comparing the cost of dispatchable concentrating solar power and photovoltaics with storage, Energy Sources B: Econ. Plan. Policy 16 (1) (2021) 55–74, https://doi.org/10.1080/15567249.2020.1843565
[207] M. Ebrahimi, Storing electricity as thermal energy at community level for demand side management, Energy 193 (2020) 116755, https://doi.org/10.1016/j.energy.2019.116755, https://www.sciencedirect.com/science/article/pii/S0360544219324508.
[208] T. Okazaki, Electric thermal energy storage and advantage of rotating heater having synchronous inertia, Renew. Energy 151 (2020) 563–574, https://doi.org/10.1016/j.renene.2019.11.051, https://www.sciencedirect.com/science/article/pii/S0960148119317380.
[209] B. Coelho, A.C. Oliveira, A. Mendes, Concentrated solar power for renewable electricity and hydrogen production from water—a review, Energy Environmental Science 3 (2010) 1398–1405, https://doi.org/10.1039/B922607A, http://dx.doi.org/10.1039/B922607A.
[210] SolarPACES, Fraunhofer Chile to develop a solar concentration system to recycle aluminum, 2023, https://www.solarpaces.org/fraunhofer-chile-to-develop-a-solar-concentration-system-to-recycle-aluminum/.
[211] N. Campion, R. Gutiérrez-Alvarez, J.T.F. Bruce, M. Münster, The potential role of concentrated solar power for off-grid green hydrogen and ammonia production, Renew. Energy 236 (2024) 121410, https://doi.org/10.1016/j.renene.2024.121410, https://www.sciencedirect.com/science/article/pii/S0960148124014782.
[212] J.P. Murray, Solar production of aluminum by direct reduction: Preliminary results for two processes, J. Sol. Energy Eng. 123 (2) (2000) 125–132, https://doi.org/10.1115/1.1351809, https://asmedigitalcollection.asme.org/solarenergyengineering/article-pdf/123/2/125/5713043/125_1.pdf.